Cell Reports

Article

Cell type specializations of the vocal-motor cortex in songbirds

Graphical abstract

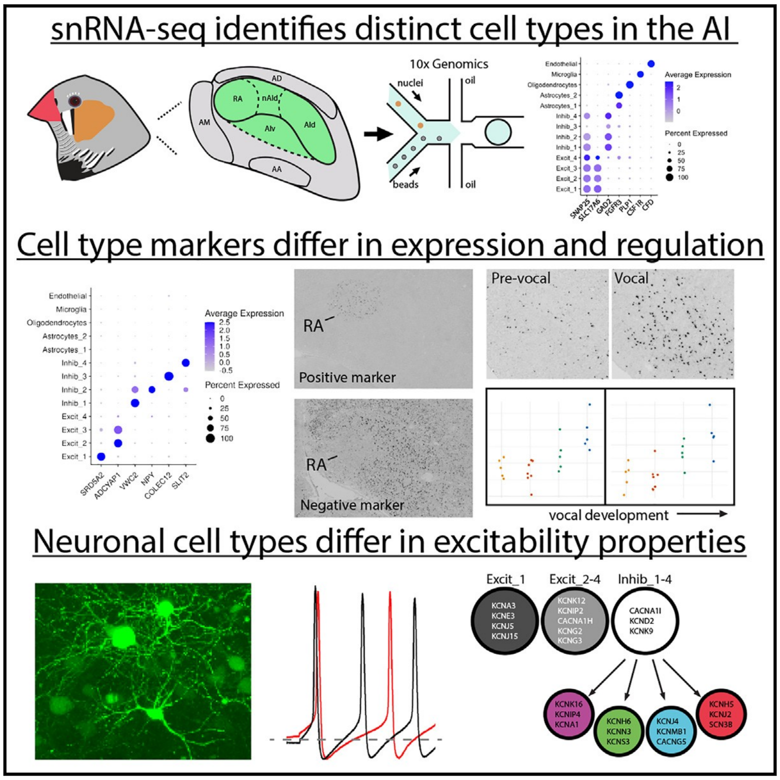

Authors

Alexander A. Nevue, Benjamin M. Zemel, Samantha R. Friedrich, Henrique von Gersdorff, Claudio V. Mello

Correspondence

vongersd@ohsu.edu (H.v.G.), melloc@ohsu.edu (C.V.M.)

In brief

Nevue et al. define cell types in the vocal robust arcopallial nucleus (RA) and adjacent areas of zebra finches based on snRNA-seq. They demonstrate neuronal and astrocyte types unique to RA and how cell-defining markers arise during vocal development. Cell type and developmental transcriptomics datasets can be easily mined with interactive applications.

Highlights

- snRNA-seq and spatial expression analysis finds cell types in RA and adjacent areas
- RA has unique excitatory neuron and astrocyte types and inhibitory neuron subtype
- Many cell type markers emerge in a sex-specific manner during vocal development
- Interactive applications created to explore cell type and developmental datasets

Nevue et al., 2023, Cell Reports 42, 113344
November 28, 2023
https://doi.org/10.1016/j.celrep.2023.113344

CellPress

Cell Reports

CellPress
OPEN ACCESS

Article

Cell type specializations of the vocal-motor cortex in songbirds

Alexander A. Nevue,[1,2] Benjamin M. Zemel,[2] Samantha R. Friedrich,[1] Henrique von Gersdorff,[2,*] and Claudio V. Mello[1,3,*]
[1]Department of Behavioral Neuroscience, Oregon Health & Science University, Portland, OR 97239, USA
[2]Vollum Institute, Oregon Health & Science University, Portland, OR 97239, USA
[3]Lead contact
*Correspondence: vongersd@ohsu.edu (H.v.G.), melloc@ohsu.edu (C.V.M.)
https://doi.org/10.1016/j.celrep.2023.113344

SUMMARY

Identifying molecular specializations in cortical circuitry supporting complex behaviors, like learned vocalizations, requires understanding of the neuroanatomical context from which these circuits arise. In songbirds, the robust arcopallial nucleus (RA) provides descending cortical projections for fine vocal-motor control. Using single-nuclei transcriptomics and spatial gene expression mapping in zebra finches, we have defined cell types and molecular specializations that distinguish RA from adjacent regions involved in non-vocal motor and sensory processing. We describe an RA-specific projection neuron, differential inhibitory subtypes, and glia specializations and have probed predicted GABAergic interneuron subtypes electrophysiologically within RA. Several cell-specific markers arise developmentally in a sex-dependent manner. Our interactive apps integrate cellular data with developmental and spatial distribution data from the gene expression brain atlas ZEBrA. Users can explore molecular specializations of vocal-motor neurons and support cells that likely reflect adaptations key to the physiology and evolution of vocal control circuits and refined motor skills.

INTRODUCTION

Understanding how complex behaviors are subserved by specialized circuits requires thorough analyses of the cell types and molecular specializations that constitute those circuits.[1,2] Investigating organisms with a well-characterized behavior and associated brain circuitry facilitates the identification of circuitry specializations when contrasted with the broader areas from which they evolved.

Vocal learning birds provide robust examples of a specialized brain circuit that supports a lineage-specific behavior.[3] In songbirds, parrots, and hummingbirds, a dedicated forebrain circuit enables the acquisition and production of learned vocalizations. The architecture of avian vocal circuits contrasts with the cortical layered organization in mammals but shares important connectivity features of cortical microcircuits.[4,5] The robust arcopallial nucleus (RA) in songbirds, an analog of the laryngeal motor cortex (LMC) in humans,[3,6] integrates inputs from premotor and corticobasal ganglia pathways of the forebrain vocal circuit (Figure 1A) and provides this circuit's sole and direct output onto vocal-motor and respiratory neurons in the midbrain and brainstem.[7,8] RA is required for singing[9] and plays key roles in modulating acoustic features of song.[7,8,10–12] RA's roles are in several ways analogous to those that corticospinal pyramidal neurons in the primate motor cortex play in the control of fine motor skills.[13] RA projection neurons are capable of firing ultrathin spikes at very high frequencies[10,12,14] due to ion channel specializations,[15,16] some of which are similar to those of the specialized Betz cells in the primate motor cortex,[17] and RA's adult firing patterns result from extensive changes during the period of song learning.[14,15,18] Despite RA's distinct physiological features and role in producing learned song, its most basic features related to cell type composition and related molecular specializations have yet to be fully defined.

RA expresses numerous molecular markers thought to reflect specialized roles in the production of learned vocalizations.[19–23] Many RA markers are convergently evolved specializations shared with other avian vocal learners (e.g., hummingbirds) and LMC in humans,[19] and a recent transcriptomics effort provided insights into molecularly defined cell types within RA.[24] For the most part, however, these studies did not examine whether the identified markers or cell type definitions might reflect broader features of cortical motor circuits. For example, roughly half of the markers shared between RA and LMC have been found in adjacent non-vocal somatic motor areas, rendering them not true RA-specific markers.[23] Considering the hypothesis that vocal-motor areas arose as specializations of more ancestral cortical motor circuits,[25] identifying differences between vocal and non-vocal motor circuitry is critical in understanding how vocal learners execute this evolutionarily rare and complex behavior.

RA is located in the intermediate arcopallium (AI), a brain region that has descending somatic projections and contains neurons considered analogous to deep-layer pyramidal cells of the mammalian motor cortex.[21,26,27] Dorsal AI (AId) is considered a motor cortical analog involved in somatic motor function[25,28,29] and broadly present in vocal learner and non-learner birds.[23] The proximity and similar involvement of RA and AId in motor function, their shared gene expression profiles, and the molecular similarities of AId between songbirds and suboscines all support the hypothesis that RA may have evolved as a songbird specialization of a more ancestral AId.[3,23,25] Ventral AI (AIv), in contrast, while also broadly present in birds, is thought to be involved in auditory processing[29–31] and has a molecular profile different from that of AId.[21] A close comparison of RA, AId, and AIv offers an excellent opportunity to identify cellular and molecular features truly unique to RA.

To define the molecular and cellular architecture of a key vocal area while considering its neuroanatomical context, we performed single-nucleus RNA sequencing (snRNA-seq) of the intermediate arcopallium, including RA, AId, and AIv, combined with *in situ* hybridization to assess the spatial distribution of the identified cell type markers. The results provide a comprehensive characterization of genes selectively enriched in RA excitatory neurons in addition to a multitude of molecular and cellular specializations unique to RA and absent in the adjacent AI. We were also able to probe the sparse GABAergic cell subtypes composition within RA using virally targeted electrophysiological recordings. To increase the utility of our datasets, we developed interactive software applications that allow integration of the cellular data with developmental transcriptome datasets[32] and with the spatial mapping of *in situ* hybridization data in the ZEBrA brain gene expression atlas.[22] These integrated resources will facilitate data mining as well as exploration of the molecular genetic basis of learned vocal behavior and the evolution of brain circuits for refined motor skills.

RESULTS

Cell type composition of the intermediate arcopallium

To determine the cell type composition of the AI in adult male zebra finches, we microdissected an area encompassing RA as well as the AId and AIv, analogous to deep-layer motor and sensory (auditory) cortices,[4,21,33] respectively (Figure S1A), and isolated nuclei for snRNA-seq[34] (Figure 1A). To avoid confounds of sensory stimulation or singing behavior, we studied quiet unstimulated birds. We identified 13 clusters representing eight classes of neurons, two classes of astrocytes (Astrocytes_1–2), and one cluster each of oligodendrocytes, microglia, and endothelial cells (Figures 1B and 1C, details in Figures S1B and S1C; full marker lists in Table S1), based on the expression of established cell type markers.[35,36] Among neuronal clusters, four were identified as excitatory (Excit_1–3, and Excit_4, which was mixed) and four as inhibitory (Inhib_1–4). There was a near 50:50 ratio in the numbers of neuronal vs. non-neuronal cells, with astrocytes being the most prevalent non-neuronal class and excitatory neurons more prevalent than inhibitory neurons (Figure 1D). Astrocytes and oligodendrocytes representing a majority of non-neuronal cells are consistent with estimations from human cortex.[37]

Because these cell clusters derived from tissue containing multiple AI subregions and spatial information is lost in snRNA-seq, we performed *in situ* hybridization for proxy genes to determine the spatial distribution of major cell classes and their proportions across AI domains. While both excitatory (SLC17A6^{+}) and inhibitory (GAD2^{+}) neurons were sparser in RA, RA exhibited higher proportions of oligodendrocytes (PLP1^{+}) and, to a lesser extent, astrocytes (ASS1^{+}) and microglia (RGS10^{+}), compared to the rest of the AI (Figures 1E, 1F, and S1D).

Excitatory neurons in the AI

The AI has diverse molecular properties and connectivity[21,23,24,29,38] including distinct electrophysiological properties of RA excitatory cells.[15,16] It is considered analogous to deep layers of the mammalian cortex, which has a large diversity of pyramidal cell types.[39] Accordingly, we detected several molecularly defined excitatory cells in zebra finch AI. Excit_1 exhibited unique markers (Figure 2A), some known to be expressed in RA only and not in other arcopallial domains.[20,22,23] *In situ* hybridization for genes with high specificity to this cluster showed expression restricted to RA (e.g., SRD5A2 in Figure 2B), supporting it as an excitatory cell type unique to RA. In contrast, genes associated with Excit_2–3 (e.g., ADCYAP1 in Figure 2D) had low to no expression in RA compared to outside the RA (Figure 2E; see also Figure S2B), noting that markers linked to Excit_3 had higher expression in AIv (e.g., CERKL in Figure S2A). Furthermore, several known negative markers of adult male RA,[22] where expression in RA is lower or lacking compared to the surrounds, were unique to or enriched in Excit_2–3 (Figure S2C). We conclude that Excit_1 is an RA-unique cluster and corresponds to the vast majority of RA excitatory neurons, commonly referred to as RA projection neurons, or RAPNs,[15] whereas Excit_2–3 correspond to excitatory cell types prevalent in AI but rare or absent in RA.

Excit_1 markers represent the first comprehensive characterization of genes selectively expressed or highly enriched in RAPNs. SRD5A2 encodes a reductase that converts testosterone into dihydrotestosterone and plays significant roles in the masculinization of RA and singing behavior.[40–42] We show that SRD5A2 expression within the arcopallium is specific to excitatory neurons in RA. Bioinformatics of the 100 most significant genes in the Excit_1 cluster found enrichment for Wnt signaling (Figure S2D), a pathway involved in brain development, neuronal maturation, and synaptogenesis.[43] Other genes encoding components of the Wnt:SFRP complex (FRZB, WNT7B, and WNT5B) were also unique to Excit_1 (Figure S2E), and RSPO3, also enriched in Excit_1, has been implicated in Wnt signaling and specification of motor neuron phenotypes.[44,45] Thus, Wnt signaling features unique to RAPNs may contribute to their differentiation from other AI excitatory neurons or to modulation of synaptic plasticity in these cells.[46] The enrichment for dopaminergic signaling was consistent with the differential expression of some dopaminergic receptors[47] and the modulatory effects of dopamine[48] in RA. Extracellular matrix receptor interaction is also of potential interest, given the involvement of the extracellular matrix in synaptic plasticity.[49] Notably, some Excit_1 markers were also markers of song nucleus HVC (abbreviation used as a proper name) (Figures S2F—S2H), a premotor input source into RA, suggesting a co-evolution of molecular markers within the vocal-motor pathway of the song circuitry.

RA undergoes major changes in morphology and gene expression during the developmental period of song learning, before reaching the sex dimorphism characteristic of adults.[32,40,41,50–56] In males, RA volume as well as neuronal soma and dendritic arborizations increase in size, whereas female RA undergoes atrophy, with decreases in volume and neuronal size and number. To

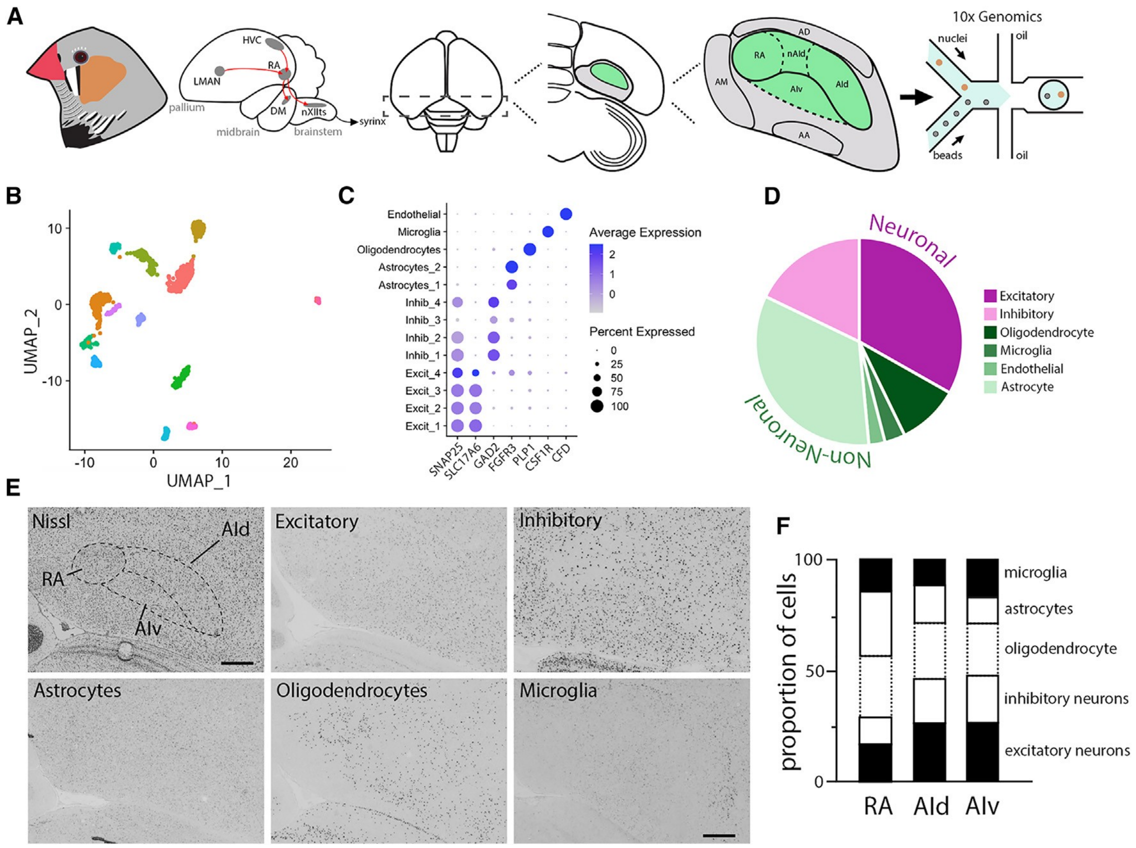

Figure 1. Cell classes of the intermediate arcopallium (AI)

(A) Workflow to generate single-nuclei transcriptomes (snRNA-seq) of AI from adult male zebra finches. Nucleus RA receives input from LMAN and HVC and projects to vocal and respiratory centers in the brainstem. Sections of the caudal telencephalon were prepared and the AI region (green) containing RA, AId, and AIv was microdissected, followed by nuclei isolation, droplet-based 10× Genomics profiling, and Illumina sequencing.

(B) Uniform manifold approximation and projection plot visualization of AI cell classes (n = 2 animals; nuclei = 1,504).

(C) Dot plot for cell type-defining genes used for cluster identity. SNAP25, neuronal; SLC17A6, excitatory; GAD2, inhibitory; FGFR3, astrocyte; PLP1, oligodendrocyte; CSF1R, microglia; CFD, endothelial. On this and similar plots in all figures, color indicates normalized expression levels and size indicates percentage of labeled cells

(D) Proportions of AI cell types from snRNA-seq: astrocytes (33.2%), oligodendrocytes (9.6%), microglia (3.2%), endothelial cells (2.5%), excitatory neurons (33.6%), and inhibitory neurons (17.8%).

(E) Nissl staining (upper left) and *in situ* hybridization images for cell type-defining genes: excitatory (SLC17A6), inhibitory (GAD2), astrocytes (ASS1), oligodendrocytes (PLP1), and microglia (RGS10). Unless otherwise indicated, *in situ* images in all other figures are from this same region of frontal sections. Scale bars, 400 mm.

(F) Proportion of each cell class across AI subdivisions from images in (E).

AA, anterior arcopallium; AD, dorsal arcopallium; AM, medial arcopallium; AId, dorsal AI; nAId, neck of the AI; DM, dorsomedial nucleus of the intercollicular complex; HVC, proper name; LMAN, lateral magnocellular nucleus of the anterior nidopallium; nXIIts, tracheosyringeal division of the hypoglossal nucleus; RA, robust nucleus of the arcopallium; AIv, ventral AI. See also Figure S1 and Table S1.

explore whether markers of the RA-unique excitatory cells (Excit_1) might be regulated during this period, we analyzed their expression within a bulk RNA-seq dataset (GEO: GSE191296) that profiled the developmental emergence of sex differences in RA gene expression.[32] Many of the genes unique to Excit_1 that are positive markers of RA in adult males increased during the period of song learning in males only (Figure 2C). This suggests that this RA-specific cell type emerges in development, concomitant with RA's sexual differentiation. In contrast, genes that define other excitatory clusters (Excit_2–3) and that are negative markers of adult male RA decreased in male RA during the period of song learning (Figure 2F), suggesting a developmental regression and/or possible loss of these cell types in males.

Given the developmental sex differences in RA growth and transcriptome,[32] it was important to examine the cell type expression of growth factor genes. Notably, the top growth-factor-related genes in the bulk RNA-seq dataset that are developmentally upregulated in male RA only were highly specific to Excit_1 (Figure 2G). The top gene in this set (ENSTGUG00000013568), an apparent LRRC32 paralog (which we refer to as LRRC32-2) and the second most enriched gene in Excit_1 (Figure 2A), results from a songbird-specific duplication of LRRC32 (Figure 2H). Whereas LRRC32-1 shares the upstream synteny with the parent gene (Figure 2H),

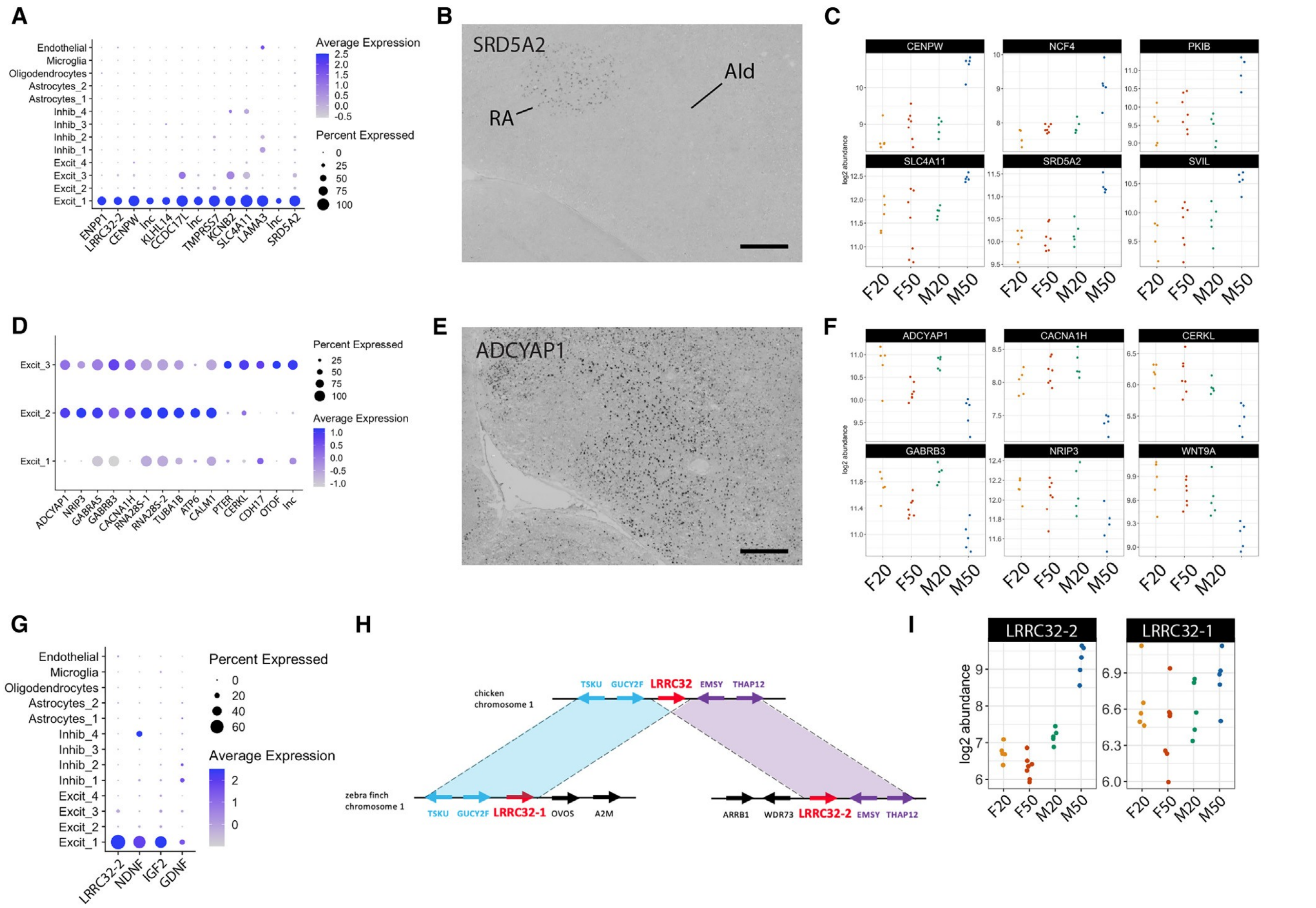

Figure 2. Molecular specializations of AI excitatory neurons

(A) Dot plot of top defining markers of cluster Excit_1.

(B) *In situ* hybridization shows that SRD5A2, a highly differential Excit_1 marker, is exclusively expressed in RA. Scale bar, 400 mm.

(C) Age and sex differences in Excit_1 marker expression; bulk RNA-seq plots show that many defining markers of this RA-specific cell type increase in males only during the period of song learning.

(D) Dot plot of the top defining markers of clusters Excit_2–3.

(E) *In situ* hybridization shows that ADCYAP1, one of the most differential markers of clusters Excit_2–3, is highly expressed in the AI but not in RA. Scale bar, 400 mm.

(F) Age and sex differences in Excit_2–3 marker expression; bulk RNA-seq plots show that many defining markers of Excit_2–3 that are low or absent in adult male RA decrease in males only during the period of song learning.

(G) Dot plot shows that growth factor genes developmentally upregulated in male RA are markers of the RA-specific Excit_1 cluster.

(H) Genomic maps of chromosome 1 in chicken and zebra finch, exhibiting the LRRC32 duplication in the latter.

(I) Age and sex differences in LRRC32 genes; bulk RNA-seq plots show that only LRRC32-2 is developmentally regulated in male RA.

Bulk RNA-seq plots in (C), (F), and (I) represent values of transcript abundance and are false discovery rate (FDR) < 0.01 for the male 20-50 comparison and FDR > 0.01 for the female 20-50 comparison, with the exception of LRRC32-1, which is FDR > 0.01 for both comparisons. Age values in (C), (F), and (I) are in days post hatch (dph). See also Figures S2 and S3.

LRRC32-2 preserves the downstream synteny and likely gained different upstream elements. Only LRRC32-2 is specific to Excit_1 and developmentally upregulated in male RA (Figure 2I), indicating that it is under different transcriptional regulation than LRRC32-1, a clear example of how two paralogs from a lineage-specific duplication differentiate, with one paralog taking on novel functions. Other growth factor genes developmentally upregulated in male RA and unique to Excit_1 are NDNF, IGF2, and GDNF (Figure 2G). IGF2 has a known distribution consistent with expression selective to RAPNs,[57] possibly supporting a growth role specific to this cell type. Overall, our strategy identified distinct excitatory cell types with diverse distributions in the AI as well as markers specific to RAPNs, many of which are developmentally regulated and possibly critical for this cell type differentiation and function.

RA is reported to have a caudodorsal (Cd) to rostroventral (Rv) topography, with the Cd projecting to the midbrain dorsomedial nucleus and/or to HVC, and the Rv projecting to medullary nuclei nXIIts/RAm in a partially myotopic fashion.[7,58] While known markers of RA show mostly a homogeneous pattern,[21,23] recent evidence suggests possible molecular differences along the Cd-to-Rv axis.[24] To further examine a molecular topography within RA, we performed bulk RNA-seq of Cd and Rv domains microdissected from parasagittal sections through the core of RA (Figures S3A and S3B). The two regions were remarkably similar in gene expression, with very few differences (Figures S3C and S3D). RA cells that project to either of its major known targets may be too sparse or not well represented in our dissections, but it is also possible that these populations are not as spatially segregated as suggested by tract tracing, noting that the full extent of these projections may not have been described. The microdissections were performed without guidance of retrogradely labeled projection neurons, which might aid in subdividing RA. While gene expression profiling of projection neurons is needed, our data suggest that RA may be more spatially homogeneous than previously suspected.

Inhibitory neurons and excitability properties in the AI

Inhibitory cells are thought to play important roles in RA physiology and in encoding acoustic features of song,[59] but little is known about their molecular properties. The four inhibitory cell types identified by GAD2 expression (Inhib_1–4; Figure 1C) differed by numerous markers selectively enriched in each subtype (Figures 3A and S4A)*In situ* hybridization of cluster-specific markers revealed differences in spatial distribution (Figures 3B, 3C, and S4B). VWC2$^+$ cells (Inhib_1) had high densities in AId and AIv but were sparse in RA, possibly contributing to the lower overall density of GABAergic cells in RA. Furthermore, based on differential expression of markers related to embryonic ganglionic eminence subdivisions, Inhib_1–4 likely have different developmental origins,[60] with Inhib_1–2 derived from the medial (MGE), Inhib_3 from the caudal (CGE), and Inhib_4 from the lateral (LGE) ganglionic eminences (Figure S4C), consistent with the data in Colquitt et al.[24] The Inhib_1 marker VWC2, sparsely expressed in adult RA (Figure 3B), showed a male-specific developmental decrease, whereas the Inhib_4 marker SLIT2 showed female-biased expression at 50 days post hatch (dph) (Figure S4D). Inhib_1–4 could also be distinguished by markers of cortical inhibitory neuron subtypes in mammals[61] (Figure S4E). Markers more highly expressed in superficial cortical layers (LAMP5 and SNCG)[62] had very low expression in Inhib_1–4 and thus seem sparsely represented in AI, whereas markers that are more evenly distributed across cortical layers (PVALB, SST, and VIP) or deep-layer biased (MEIS2) were more highly expressed in AI, with levels differing across clusters (Figures S4E and S4F). This is consistent with the notion that the avian AI, or at least some of its neuronal populations, is analogous to deep cortical layers in mammals.[21] Parvalbumin (PVALB), a calcium-binding protein and classical marker of cortical inhibitory neurons in mammals, was expressed in both excitatory and inhibitory neurons (Figures S4G and S4H), consistent with the high density of PVALB$^+$ cells in RA (and other song nuclei) from mRNA and protein profiling.[21–23,63–65] PVALB is thought to facilitate fast spiking in mammalian interneurons and may subserve a similar function in RAPNs, which have high spiking capabilities.[15]

Based on GAD2 *in situ* hybridization of adult male RA and consistent with previous reports,[22,66] we observed GABAergic cells with large and small somata, the latter being more prevalent (Figure 3D, right). Both morphotypes were also observed in other pallial song nuclei, the large somata appearing larger than any GAD2$^+$ cells outside of song nuclei (Figures S4I and S4J). In contrast to adults, GAD2$^+$ somata in RA appeared uniformly small in 20-dph males (Figure 3D, left; quantifications in Figures 3E and 3F). Importantly, NPY$^+$ cells (Inhib_2) inside RA but not in the adjacent AId included both large and small soma subtypes (Figures 3G and 3H), whereas cells labeled for markers of all other inhibitory clusters were uniformly small. These findings suggest that the large soma GABAergic cells in RA correspond to a subtype of NPY$^+$ cells and that the soma size of this NPY$^+$ cell subset in RA increases during the developmental vocal learning period.

RA inhibitory neurons have been described as fast-spiking interneurons (FSIs) with narrow action potential (AP) half-width and small soma,[67,68] but due to their sparseness they remain poorly characterized. Given the molecular and morphological diversity we observed in RA, we sought to determine whether their electrophysiological profiles were also diverse or conformed to the FSI categorization. To make targeted recordings, we injected AAV-mDlx-eGFP,[69] which selectively labels forebrain inhibitory neurons, into RA of adult male zebra finches. As with *in situ* hybridization, GFP-labeled cells had both large and small somata (Figure 4A). We then measured passive properties of GFP$^+$ neurons ($n = 24$) using sequential negative current injections in the whole-cell current-clamp configuration. We observed that cells with high input resistance displayed larger spontaneous postsynaptic potentials (PSPs) compared to cells with low input resistance (black and red traces in Figure 4B, respectively). To eliminate contamination from spontaneous APs, we measured PSP amplitudes during current injections of 150 pA. Small cells produced significantly larger-amplitude PSPs than large cells (mean ± SE: 2.57 ± 0.15 mV, $n = 94$ PSPs for small cells and 1.42 ± 0.09 mV, $n = 31$ PSPs for large cells; Mann-Whitney U test, $p = 3.9 \times 10^{-10}$, $U = 447.5$). The membrane potentials from which the PSPs were measured were statistically indistinguishable between the two cell types, with averages of 94.75 ± 5.87 mV and 87.43 ± 5.87 mV (mean ± SE) for small and large cells, respectively. We additionally observed a broad range of input resistance values and a more limited range of membrane time constant values (Figure 4C). Upon calculating the membrane capacitance (C_m), a proxy for surface area, we observed cells with low and high C_m values (black to red gradient in Figure 4C). When plotting C_m values in a frequency histogram, we observed two distinct peaks that could be fitted with a double Gaussian, with a greater proportion of cells exhibiting low C_m (Figure 4D). We interpret the low and high C_m peaks as corresponding respectively to the small and large soma GABAergic cells observed by *in situ* hybridization for GAD2 (Figure 3D, right) and confocal imaging of GFP$^+$ cells (Figure 4A).

We next measured spontaneous and evoked APs and performed a principal component analysis of passive and active membrane property measurements of RA GABAergic cells. The large soma/high C_m cells clustered tightly together, whereas the small soma/low C_m cells were more diverse and spread out (Figure 4E, red and black dots, respectively). This difference likely reflects our identification of a single large soma subtype compared to multiple small soma subtypes. Small soma/low C_m cells were more often spontaneously active than large soma/high C_m cells (Figure 4F). When superposing all AP waveforms and derived phase plots of those waveforms recorded

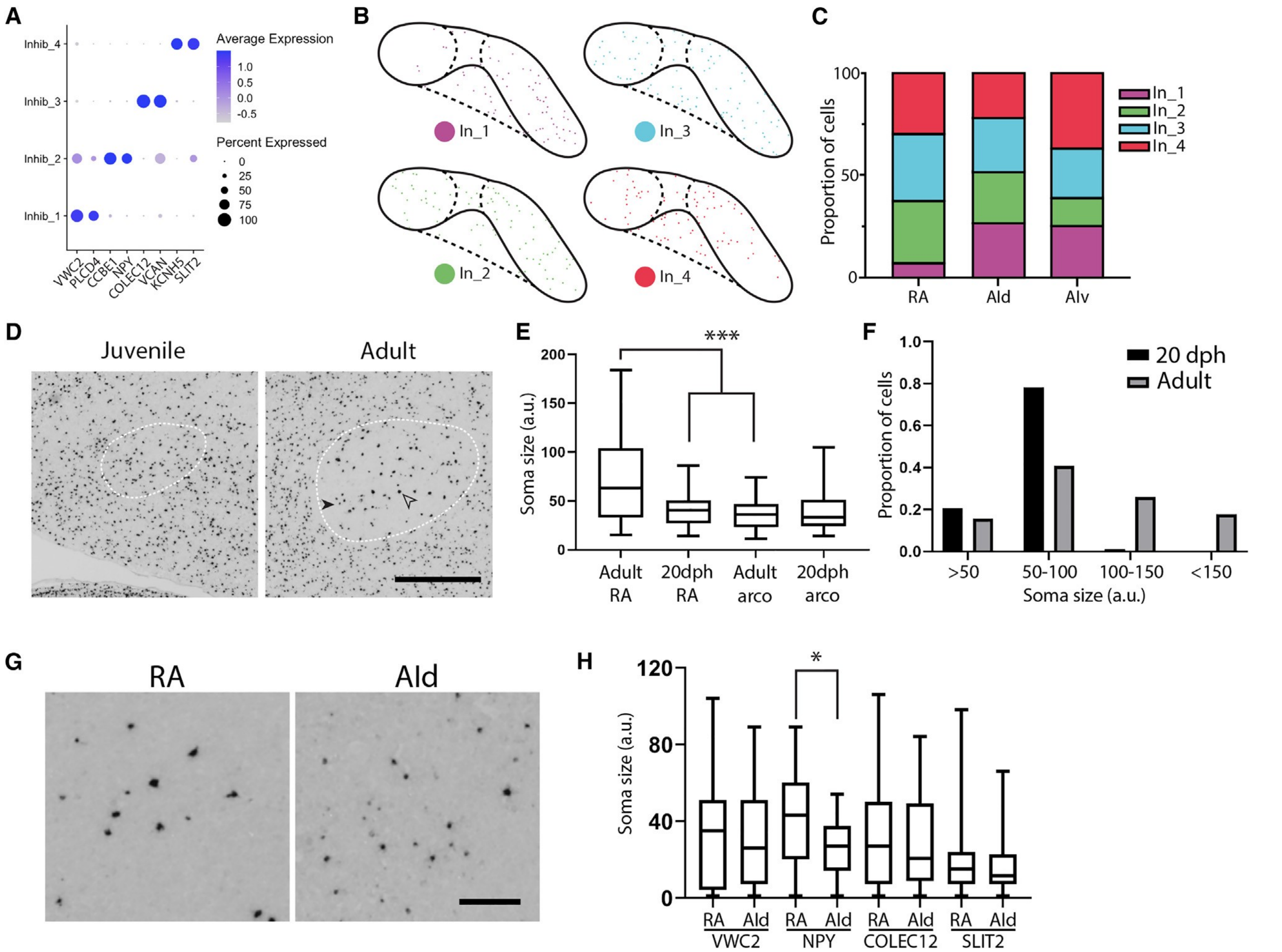

Figure 3. Inhibitory subtypes of the AI

(A) Markers that differentiate the four GABAergic neuron subtypes.

(B) Spatial distribution of inhibitory subtypes based on mapping of *in situ* hybridizations for VWC2 (Inhib_1), NPY (Inhib_2), COLEC12 (Inhib_3), and SLIT2 (Inhib_4); corresponding images in Figure S4B.

(C) Quantification of spatial distribution of inhibitory subtypes; plotted are the proportions of cells from each subtype per AI subdivision.

(D) GAD2 *in situ* hybridization of RA (white border) in juveniles (20 dph) and adult males. Open arrow denotes example of large soma $GAD2^+$ morphotype; closed arrow denotes example of small soma $GAD2^+$ morphotype. Scale bar, 400 mm.

(E) Quantification of $GAD2^+$ soma size in RA and in the caudal arcopallium outside of RA (arco) in juvenile (20 dph) and adult males. Adult RA vs. 20 dph RA, $p < 0.0001$; adult RA vs. adult arco, $p < 0.0001$; 20 dph RA vs. 20 dph arco, $p = 0.9596$.

(F) Counts of $GAD2^+$ cells of different soma sizes in juvenile (20 dph) and adult male RA. The larger somata are notably absent in juveniles. Adult vs. 20 dph RA, $p < 0.0001$.

(G) *In situ* hybridization for NPY reveals two morphotypes in RA but not in AId. Scale bar, 100 mm.

(H) Quantification of soma size of inhibitory subtypes in RA and AId. VWC2 RA vs. AId, $p = 0.8679$; NPY RA vs. AId, $p = 0.0814$; COLEC12 RA vs. AId, $p = 0.9804$; SLIT2 RA vs. AId, $p = 0.9804$.

Shown in (E) and (H) are the median, 25th and 75th percentiles (box), and maximum and minimum values; shown in (F) are average values.

***$p < 0.0001$, *$p < 0.1$ following one-way ANOVA multiple comparisons. n = 3–4 animals per condition. See also Figure S4.

during a +100 pA current injection, there was considerable variability and no consistent differences among inhibitory subtypes (Figure 4G). Importantly, the AP waveforms in all recorded neurons, regardless of C_m values, were highly reminiscent of those previously described in RA interneurons,[15,67,68,70] with narrow half-widths and sharp slopes of the rising phase following the peak of the afterhyperpolarization (Figure 4H). While there was a trend for a higher instantaneous firing frequency between the first two spikes of an evoked AP train in small compared to large cells (Figure S5A), when pooling data from all spikes throughout the current injection small cells showed significantly higher firing frequencies than large cells (Figure 4I). Of note, we observed highly variable firing rates during spontaneous and evoked firing among interneurons of both subtypes (Figures S5B and S5C) compared to the regular, periodic firing typical of RAPNs[15] (Figure S5D).

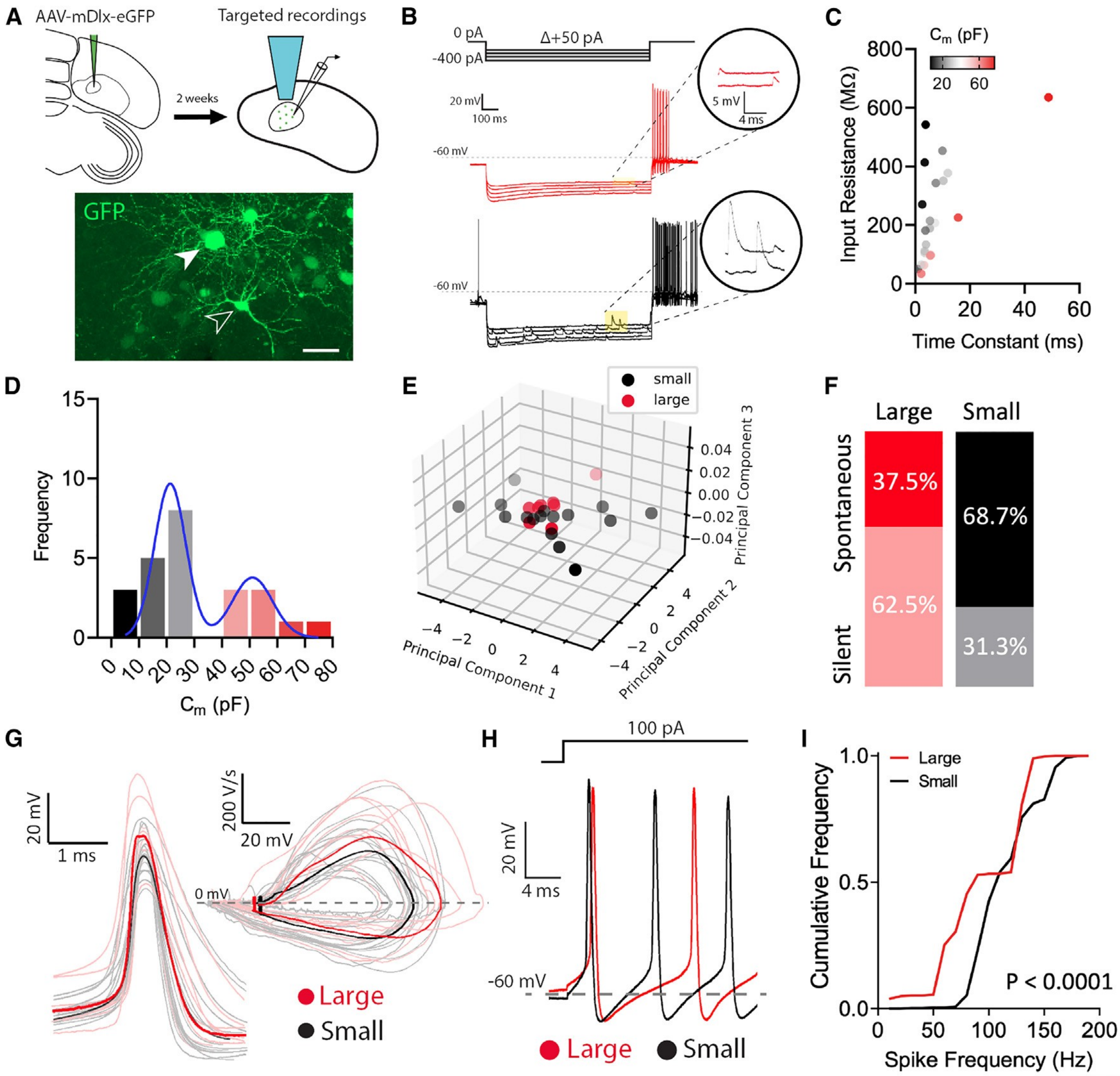

Figure 4. Electrophysiological characterization of GABAergic interneurons in RA of adult males

(A) GABAergic cells in RA slices. AAV-mDlx-eGFP was injected into RA (top left); after adequate survival, targeted recordings of GFP$^+$ cells (n = 24 total) were performed (top right). Image of slice from injected brain (bottom) shows representative examples of small soma (open arrowhead) and large soma (closed arrowhead) neurons in RA. Scale bar, 20 mm.

(B) Representative recordings of responses to negative current injections (top) in cells with high (black traces, bottom) or low (red traces, middle) input resistance. Shown are five overlaid example traces with different levels of current injected used to calculate capacitance (C_m). Insets of highlighted (yellow) regions in the traces show that larger mini PSPs are detected during current injections in cells with high (black traces) vs. low (red traces) input resistance.

(C) Graph plotting the input resistance vs. the time constant of recorded GFP$^+$ cells; dot color indicates the C_m values of the individual neurons.

(D) Frequency distribution histogram of calculated C_m for all GFP$^+$ cells recorded; bins = 10 pF. Histogram was fit by two Gaussian curves revealing distinct populations of neurons as determined by the calculated C_m.

(E) Principal component (PC) analysis of passive and active membrane properties of recorded cells. PC1 accounted for 31.7% of the variance, PC2 accounted for 23.0%, and PC3 accounted for 13.1%.

(F) Proportions of large vs. small cells that were spontaneously active.

(G) Overlays of average action potential waveforms (left) and phase plots (right) for all large and small GFP$^+$ cells recorded during a 1 s +100 pA current injection; solid red and black traces are the average waveforms and phase plots for each cell subtype.

(H) Overlay of recordings in large (red trace) and small (black trace) neurons during the first 24 ms of a +100 pA current injection.

(I) Cumulative distributions of firing frequencies from large (red) and small (black) cells. Kolmogorov-Smirnov test, D = 0.4126, n = 289 large cell events and 1,044 small cell events.

In (E)–(I), large soma/high C_m cells are labeled in red, and small soma/low C_m cells are labeled in black. See also Figure S5.

Having obtained detailed electrophysiological recordings of inhibitory interneurons, we next examined whether any molecular correlates of excitability might help explain differences between the recorded properties of inhibitory vs. excitatory cells, or among inhibitory subtypes. We found marked differences for low-threshold voltage-gated potassium channels, with the almost exclusive expression of KCND2 (Kv4.2) subunits in inhibitory neurons (Figure S5E) contrasting with excitatory neurons as a group expressing more KCNB1 and KCNB2 (Kv2.1 and Kv2.2) subunits. The difference in the inactivation properties of these channels, with Kv4.2 exhibiting profound inactivation compared to Kv2.1 and Kv2.2,[71,72] may in part explain the contrast in the slope of the afterhyperpolarization of APs between AI inhibitory vs. excitatory neurons.[15,16,67,70] Other ion channel subunit genes (Figures S5E and S5F) with expression unique to or enriched in inhibitory cells (e.g., CACNA1I, KCNK2/9) contrast markedly with those enriched in excitatory cells generally (e.g., KCNA10, CACNA2D4, SCN4B), in RAPNs (Excit_1) alone (e.g., KCNJ5) or in other AI excitatory cells (e.g., CACNA1H, KCNG1/3, KCNH4), but possible links to differences in AI cell excitability remain to be defined. As for inhibitory subtypes, expression of KCNN3, which encodes a small-conductance calcium-dependent potassium channel (SK3), was almost exclusive to a small proportion of cells in the Inhib_2 cluster (NPY$^+$; Figure S5F), which contains the large-diameter interneurons. SK channels have been shown to prolong interspike periods in numerous cell types through increasing the potassium conductance during those periods.[73] The differential expression of this channel may therefore help explain the lower firing frequency in large vs. small interneurons. Furthermore, given that the APs recorded from all interneurons taken together were highly variable (Figure 4G), it is noteworthy that many ion channel genes that can directly affect membrane excitability differed considerably in expression across inhibitory subtypes (Figure S5G). Several others were found to be enriched in specific subtypes, for instance KCNIP4 and KCNK16 in Inhib_1, KCNS3 in Inhib_2, KCNJ4 and CACNG5 in Inhib_3, and KCNH5 and SCN3B in Inhib_4 (Figures S5E and S5F). While direct links to cell type differences in excitable properties require pharmacological or genetic manipulations, these findings (summary in Figure 7F) highlight the utility of our molecular dataset in identifying molecular targets and testable predictions for how excitability is shaped within the AI.

Non-neuronal cells

Non-neuronal cells also exhibited specializations in RA. *In situ* hybridization for the oligodendrocyte marker PLP1 showed marked enrichment in RA (Figure 1E). Other known oligodendrocyte markers in mammals were unique to the PLP1-defined cluster (Figure 5A), and UGT8 and other candidate oligodendrocyte markers in ZEBrA[22] with a similar enriched expression in RA as PLP1 were also highly specific to this cluster (Figure 5A). UGT8$^+$ cells inside RA were small, with scant strongly labeled cytoplasm (Figure 5B, bottom), similar to the UGT8$^+$ cells seen at high densities in occipitomesencephalic fiber bundles and tract (Figure 5C, bottom right). UGT8$^+$ cells were also prevalent along the fiber tract connecting song nuclei HVC and RA (Figure 5C, bottom left), consistent with the heavily myelinated song system projections,[74] and in avian analogs of thalamo-recipient layer 4 of mammalian sensory cortices (Figure S6), which are also heavily myelinated.[75] A preponderance of labeled cells for UGT8 and other genes unique to or enriched in the PLP1-defined cluster was also seen in the other pallial song nuclei compared to adjacent areas (Figure 5C, top). These findings strongly support this cluster as representing oligodendrocytes, indicate that oligodendrocytes are enriched in pallial song nuclei, and define highly enriched molecular markers for this cell type in songbirds.

Of the markers that defined astrocytes, many were shared between Astrocytes_1–2, including classical markers (e.g., EGF, FGFRL1), whereas Astrocytes_2 exhibited additional markers absent in Astrocytes_1 (Figure 5D). Expression of a shared Astrocytes_1–2 marker (ASS1) was broadly distributed throughout the AI (Figure 1E), whereas expression of CRISPLD1, a highly differential gene in the Astrocytes_2 cluster, was restricted to RA and absent in AId (Figure 5E). This distribution suggests that Astrocytes_1 is broadly distributed in the AI, whereas Astrocytes_2 is largely restricted to RA. Cells expressing CLIC4, a gene highly enriched in the endothelial cell cluster (Figure 5F), were also at a higher proportion in RA (Figure 5G).

Examination of the developmental RNA-seq dataset[32] revealed that most of the genes upregulated in both male and female RA during the period of song learning were associated with the oligodendrocyte cluster (Figures 6A and 6B). This suggests that oligodendrocyte-related functions are an intrinsic feature of RA development, regardless of sex and vocal development. This is surprising, given that female zebra finches do not sing and female RA shows developmental decreases in volume as well as neuron size and number.[50,52] *In situ* hybridization for PLP1 confirmed this finding, with a developmental increase in both male and female RA indicating increased density of oligodendrocytes in both sexes (Figure 6C). A developmental increase in myelination within and across song nuclei has previously been described in males,[74] but the present results suggest this increase is not specific to males. Lastly, genes associated with the endothelial cell cluster increased in expression during development only in male RA (Figures 6D and 6E). Besides assigning an endothelial identity to these developmentally regulated genes, our findings support the notion that a higher capillary density to meet the metabolic demands of high-frequency firing distinguishes RA neurons in adult males compared to juveniles and females, as previously suggested.[32,76]

Insights into RA physiology gene expression: Neurotransmission, connectivity, and transcriptional regulation

To gain further insight into physiological specializations of AI cell types, we examined the expression of genes involved in fundamental neuronal processes such as synaptic transmission/modulation, connectivity, molecular transport systems, and transcriptional regulation (Figure S7). Excitatory cells predominantly expressed various GABAergic and serotonergic receptor classes and primarily expressed some dopaminergic (DRD3) and cholinergic (CHRM5) receptors, with RA-specific Excit_1 primarily expressing GABRE, whereas inhibitory cells primarily expressed other GABAergic subunits, with Inhib_2 primarily expressing GABRG1, CHRM2, and DRD2 (Figure S7A). These findings

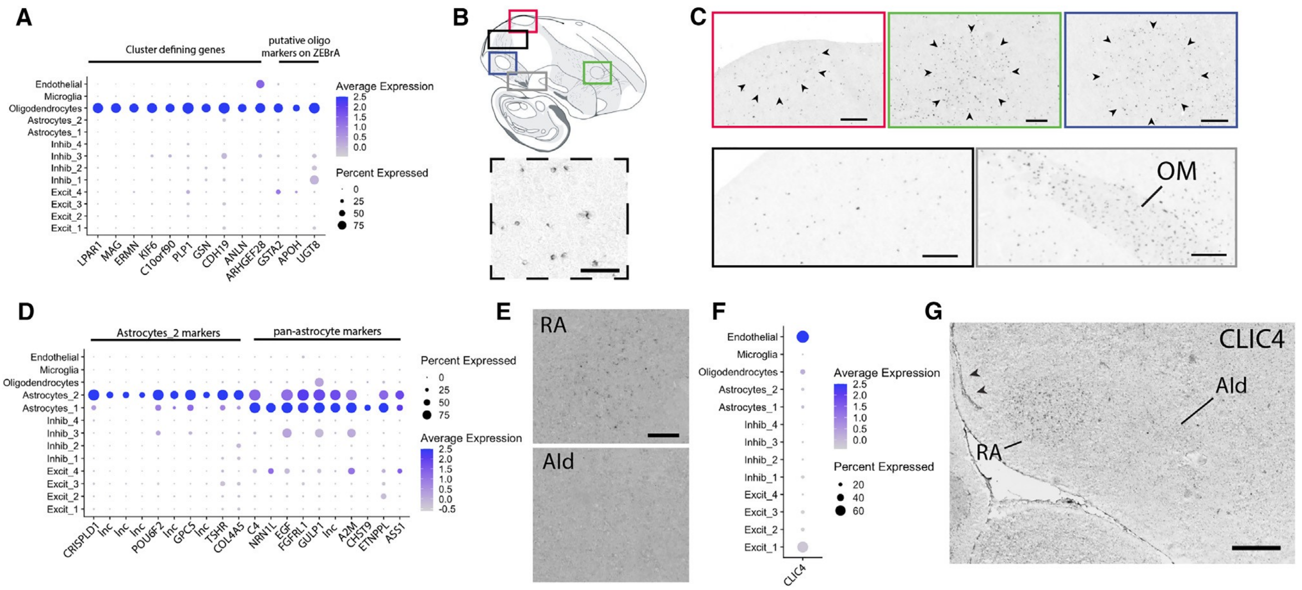

Figure 5. Non-neuronal specializations in song nuclei of adult male zebra finches

(A) Dot plot with top differentially expressed genes in the oligodendrocyte cluster and putative oligodendrocyte markers on ZEBrA based on expression patterns.

(B) Top: drawing of parasagittal section with forebrain song nuclei and fiber tracts (adapted from ZEBrA: www.zebrafinchatlas.org[22] and from[75]); areas in colored rectangles are shown in (C). Bottom: *in situ* hybridization for UGT8 (from ZEBrA) shows cellular expression pattern in RA consistent with oligodendrocytes.

(C) *In situ* hybridization for UGT8 (from ZEBrA) shows oligodendrocyte enrichment in pallial song nuclei HVC (red), LMAN (green), and RA (blue) compared to surrounds. Bottom panels show views of the fiber tract from HVC to RA (black) and the occipitomesencephalic tract (OM) (gray); rectangle locations shown in (B).

(D) Dot plot with top differentially expressed genes in the astrocyte clusters.

(E) *In situ* hybridization for CRISPLD1, an Astrocyte_2 enriched gene, shows higher density of labeled cells in RA (top) compared to AId (bottom).

(F) Dot plot for CLIC4, a gene enriched in endothelial cells.

(G) *In situ* hybridization image for CLIC4 in frontal section shows higher density of labeled cells in RA than elsewhere in the AI.

Arrowheads indicate expression in ventricle. Scale bars, 100 mm in (B) (bottom left); 400 mm in (C), (E), and (G). See also Figure S6.

indicate different synaptic specializations of various cell types and provide a cellular basis for the differential expression of various neuromodulatory receptors in RA,[20,77–80] insights into likely cellular target of action of related drugs known to affect RA physiology,[48,78,81–84] and predictions for cell type-specific effects for future pharmacological studies. As for axonal guidance and connectivity, several genes were differential in excitatory (e.g., ADCYAP1, SEMA3F, CDH17, DCN) vs. inhibitory (e.g., SLIT2, RELN, SEMA3A/C/E, UNC5C) cells (Figure S7B). We note the selective expression of DCN in RA-specific Excit_1 and of RELN in Inhib_1–2, consistent with these genes being robust positive and negative markers of RA, respectively (*in situ* patterns in ZEBrA; see also[85]).

For transcription factors, we focused on those with defined DNA-binding motifs and that are developmentally regulated in RA during the period of song learning.[32] Several transcription factors were differential across cell types (Figures S7C and S7D), noting the selective expression of NKX2-8 in RA-specific Excit_1, ZBTB7C and ETV4 in Inhib_3, HEY2 and PAX6 in astrocytes, NKX6-8 in oligodendrocytes, and LEF1 in endothelial cells. Intriguingly, the speech-linked FOXP2 gene, expressed at low levels in RA,[86] was primarily associated with inhibitory neurons and endothelial cells, not principal excitatory cells. Immediate-early genes (EGR1, CFOS, and CJUN) were mostly expressed in non-neuronal cells, consistent with the birds being quiet and unstimulated around sacrifice and supporting this dataset as constitutive rather than reflecting activity-inducible expression. Lastly, several transporter genes (SLCs) showed expression restricted to neurons vs. astrocytes (the latter for metabolites such as succinate, citrate, or bicarbonate) or in excitatory (SLC17A6) vs. inhibitory (SLC32A1) cells (Figures S7E—S7F). We note the selective expression of a glycine transporter (SLC6A9) in Excit_4, which could be associated with local glycinergic transmission,[87] and of the glucose transporter (SLC2A1) in endothelial cells, consistent with a brain sugar transport role of this cell type.[88] The identified cell types thus exhibit specialized molecular features associated with fundamental aspects of neuronal physiology, connectivity, and transcriptional regulation. These findings provide an important basis for future studies using neurophysiology, pharmacology, and molecular genetics to assess gene function.

Interactive applications for data exploration

To enable further exploration of RA cell properties, we have developed data visualization applications that allow rapid assessment of cell type and sex/developmental gene expression data from RA snRNA-seq and bulk transcriptome datasets and have integrated them with *in situ* hybridization data from ZEBrA (www.zebrafinchatlas.org) for assessment of spatial gene expression patterns (Figures 7A–7D). This allows one to examine the brain distribution of genes selectively expressed in specific cell types or developmentally regulated in one or both sexes or, conversely,

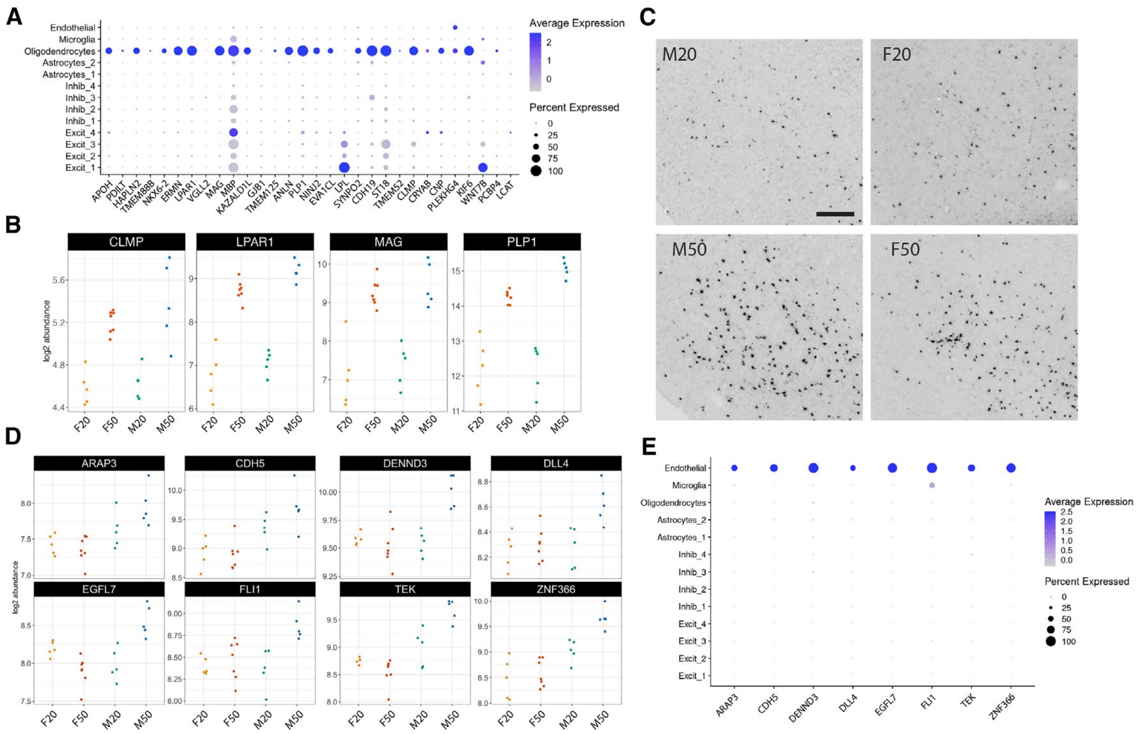

Figure 6. Developmental changes in non-neuronal composition in RA

(A) Most genes that increase in RA in both males and females [32] are highly enriched in the oligodendrocyte cluster.

(B) Developmental gene expression plots for four highly specific oligodendrocyte markers from (A).

(C) *In situ* hybridization for PLP1 showed increased developmental expression in RA in both sexes; labels represent age in dph. Scale bar, 250 mm.

(D) Endothelial cell markers show a male-specific developmental increase in expression.

(E) Dot plot for endothelial cell markers shown in (D).

Bulk RNA-seq plots in (B) and (D) are FDR < 0.01 for the male 20-50 comparison and FDR > 0.01 for the female 20-50 comparison.

the RA cell type specificity or developmental profiles of RA marker genes in ZEBrA. As examples, genes expressed in Excit_1–4 (GABRA5) or in all neuronal cell types (FLRT2) show expression and/or enrichment in RA, but those specific to Excit_2–3 (CACNA1H) or Inhib_1–3 (RELN)are restricted to the AI outside of RA (Figure 7A), consistent with Excit_1 being RA specific but Excit_2–3 and Inhib_1 being largely absent in RA.

We also plotted how the most differentially expressed cell-cluster-defining markers are regulated in the sex and age contrasts of the developmental dataset. Numerous markers of GABAergic subtypes and of excitatory neurons that are sparse or absent in adult male RA (Excit_2–3) were developmentally downregulated in young males, their expression becoming female biased by 50 dph (Figure 7B, bottom, middle, and right panels), whereas several markers of the RA-specific Excit_1 showed a developmental increase, mostly in males, and were male biased at 50 dph (Figure 7B, bottom, red color). Markers of the RA-specific Astrocytes_2 and of endothelial cells increased primarily in males (Figure 7B, top, middle, and right panels), whereas oligodendrocyte markers were markedly upregulated in both males and females (Figure 7B, top, left, and middle panels), in agreement with PLP1 expression (Figures 6B and 6C).

These examples illustrate how the incorporation of our interactive applications to the ZEBrA atlas (Figures 7C and 7D) allows the rapid examination of cell type specificity, developmental regulation, sex differences, and brain distribution of molecular markers of a major song nucleus. These integrated resources thus enhance the opportunities for data mining and formulation of testable hypotheses on gene regulation and function within the zebra finch vocal circuitry.

DISCUSSION

We presented here a characterization of molecularly defined AI cell classes and their distribution in zebra finches and identified molecular specializations linked to basic functions such as excitability, connectivity, and transcriptional regulation of these cell classes. The AI is a complex region that includes song nucleus RA, whose projection neurons are analogous to pyramidal cells in human LMC, and the adjacent AId and AIv, considered analogous to deep layers of mammalian somatic motor and auditory cortices, respectively.[33,89] While several cell classes were broadly distributed, our spatial analysis provides support for the existence of specialized cell types within RA (Figure 7E). This includes an excitatory neuron, a large inhibitory subtype, and an astrocyte unique to RA, as well as evidence of high enrichment of oligodendrocytes in RA, noting that RAPNs project to brainstem via heavily myelinated axons that support

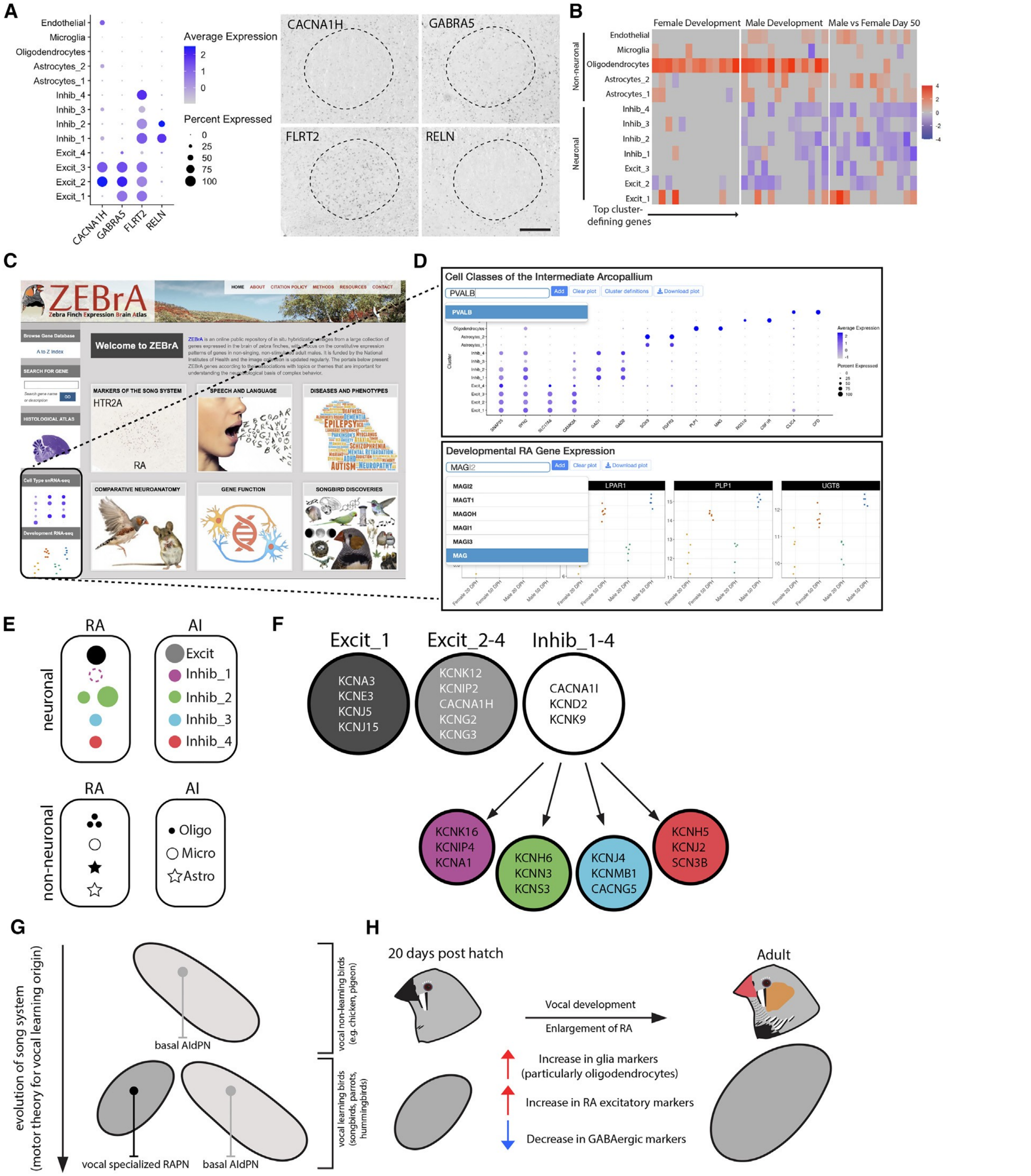

Figure 7. Integration of spatial distribution and cell expression data and summary of RA cell types

(A) Cell type expression data provide insights into gene expression patterns seen by *in situ* hybridization; in the examples shown, cell class distributions (left) help explain differential expression of positive and negative RA markers (right; *in situ* hybridization data from ZEBrA: www.zebrafinchatlas.org).

(B) Integration of cell type and developmental datasets reveals sex- and age-dependent regulation of specific RA cell type markers. Plotted is the $\log_2$ fold change for the top cluster-defining genes in each comparison; for age comparison, 20:50 dph ratios; for sex comparison, male/female at 50 dph ratios. Scale bar, 500 mm.

(C) R Shiny applications to interact with the datasets presented in this study are linked on the homepage of ZEBrA; image adapted from[22].

(D) Examples of using the applications depicted in (C) for assessment of cell type (top) and sex/age developmental (bottom) profiles in RA.

(legend continued on next page)

fast-propagating spikes. These findings reflect fundamental properties of the song circuitry and the specialized physiology of RA at the single-cell level, noting that the data provide evidence of cell type specificity for numerous genes. More broadly, the findings bring insights into the organization and evolution of specialized brain regions for complex learned behaviors.

By including multiple AI regions, our study provided neuroanatomical context to the cellular transcriptome analysis of RA. This approach, previously used in an extensive *in situ* hybridization study of RA markers,[23] allowed the identification of specializations truly unique to RA, i.e., not shared by neighboring AI regions. While the study by Colquitt et al.[24] had a goal of defining cell subtypes exclusively within RA, the assessment of anatomical context, as done here, allows for both a confirmation of the spatial location of specific cell types and the identification of features unique to RA. Based on our data, we note that markers of putative RA excitatory neuron subtypes identified by Colquitt et al.[24] are also highly expressed outside of RA (e.g., CRHR2, NFATC1) or in non-excitatory neuron populations (e.g., ADAMTS18, RUNX1) (Figure S7G). These findings illustrate the critical need for regional comparisons, a concept which we refer to as molecular context and which will be key in the rapidly developing spatial genomics landscape.[90]

Our data clearly show that the major projection neurons in RA (Excit_1) express markers not expressed in other AI regions. Their identification addresses an important gap, as the majority of known markers specific to RA were negative ones.[22,23] Genes selective to RA projection neurons likely reflect proteins that are active within these cells and thus poised to affect their growth, differentiation, and firing behavior. This includes mediation of spectral features of song through patterned burst-pause type firing,[10,12] a function possibly modulated by GABAergic interneurons[59] and by regulators of intrinsic excitability[15,16] and synaptic transmission in RA. The identified molecular features of RA-specific projection neurons and the diverse interneuron subtypes provide a solid basis for hypothesis-driven mechanistic studies of gene function in the context of vocal circuits.

Zebra finch RA is highly dimorphic, its large projection neurons subserving song production in males, whereas in females, which do not sing, RA undergoes marked developmental reductions in volume and in neuron number and size.[40,50,52,53] Integration of our single-cell data with bulk developmental RNA-seq datasets[32] revealed that many cell type markers of adult RA are developmentally regulated during the period of song learning in a sex-specific manner. In particular, many markers of the RA-specific Excit_1 are developmentally upregulated in males only, whereas markers of cell types absent in adult male RA are downregulated in males and/or upregulated in females during this same period. These findings provide an indication that excitatory cells differentiate during the developmental period of song learning in a sex-specific manner, with implications for understanding the ontogenesis of RA as a specialized song nucleus that differs in morphology and firing patterns between males and females.[15,52] Notably, adult male RAPNs express a set of ion channel genes that allows them to exhibit narrow APs with high-frequency firing, including KCNC1/2 (Kv3.1/3.2), SCN8A (Nav1.6), and the modulatory subunits SCN1B (Navb1) and SCN4B (Navb4), the latter promoting resurgent Na^+ currents in RAPNs.[15,16,91] These genes are also consistently found in the axon initial segment and/or nodes of Ranvier of central nervous system fast-spiking neurons and axons including those of auditory[92] and vestibular neurons,[93] and have been suggested to be part of a ‘‘fast-spiking gene module’’ that enables rapid and resilient spiking.[93]

The developmental growth of RA in males is largely dependent on the actions of sex steroids, particularly estradiol.[41] We found that many cell type markers of adult RA undergo changes during RA’s developmental growth period (summarized in Figure 7H). Notably, the enzyme encoded by SRD5A2, one of the most differential markers of Excit_1, converts testosterone into 5-a-dihydrotestosterone (5a-DHT), which potentiates the actions of estradiol and is required for the full masculinization of RA and the full expression of male singing behavior.[94,95] SRD5A2 is one of the most specific RA markers to date by *in situ* hybridization, and it is developmentally upregulated in males only. Its cell specificity indicates that RA projection neurons are the site of local 5a-DHT production, which then can act directly on androgen receptors in RA.[56] Other genes related to growth and differentiation and selectively expressed in Excit_1 are developmentally upregulated in male RA only and could contribute to the growth and differentiation of RA. This includes a novel paralog of a growth factor gene (LRRC32) that is a key regulator of the transforming growth factor b pathway,[96] a transcription factor linked to early development of the nervous system (NKX2-8),[97] and several genes linked to Wnt signaling.

During development, the axons of RA projection neurons are likely guided by a combination of attractive and/or repulsive guidance molecules to establish their connections.[7,8] Identifying the cell specificity of axonal guidance genes provides well-informed hypotheses on the connectivity regulation of projection neuron in RA and other AI regions. Furthermore, while parts of the zebra finch pallium and mammalian cortex may be divergent in origin,[24] their convergent expression of markers can give clues to the function of specific populations of arcopallial neurons. For instance, KLHL14, highly enriched in Excit_1 cells, was recently identified as expressed in a specific population of mouse primary motor cortex neurons, its deletion causing axons to extend into the spinal cord past their brainstem targets.[98] KLHL14 could

(E) RA excitatory neurons had a specialized gene expression profile that differed from those in AId. Similar GABAergic subtypes were present in RA and AId, but in RA Inhib_1 had a lower density, and a subset of Inhib_2 had large soma. Non-neuronal differences included greater numbers of oligodendrocytes in RA and an RA-specific astrocyte subtype.
(F) Summary of major cell types and subtypes found in RA and AId, and respective sets of genes linked to cell excitability.
(G) RA is hypothesized to have evolved as a specialization of preexisting AId, RA projection neurons (RAPNs) arising via specialization of existing AIdPNs.
(H) Changes in RA cell type markers during vocal development. With an enlargement of RA in males, we observe increases in some RA excitatory markers and non-neuronal markers and a decrease in GABAergic markers. These specializations may contribute to the physiology of producing learned vocalizations.
Note that schematics are not to scale.

thus be an important determinant of specific connections of Excit_1 to the brainstem. ADCYAP1, in contrast, enriched in AI excitatory clusters that predominate outside of RA and a robust negative RA marker, is a marker of deep-layer corticopontine/corticospinal neurons in the mouse,[39] consistent with the projections and function of the AI, particularly AId.[38] SLIT2 was exclusively expressed in inhibitory neurons in the AI, whereas SLIT1 and the SLIT receptors ROBO1 and ROBO2 were found predominantly in RA inhibitory cells as well as in excitatory cells that are sparse in RA. These findings are inconsistent with the suggested involvement of SLIT-ROBO signaling in establishing the long-range connections between RA and nXIIts/RAm.[99] Instead, our data suggest that SLIT-ROBO mechanisms are more likely involved in establishing local inhibitory networks in RA.

There is solid evidence that GABAergic neurons may regulate RA projection neuron spiking behavior,[59,67,68,100] but our study considerably expands the limited knowledge of interneuron properties and diversity within RA. Even though the proportions and molecular identities of inhibitory neuron types may be largely conserved across brain regions,[24] the lower density of GABAergic neurons in RA compared to the rest of the AI seems largely due to the lack of Inhib_1 cells in RA. Furthermore, while we found small FSIs, as previously described,[67] we also found sparser, larger GABAergic cells that do not conform to the canonical small FSI classification. These large cells seem to originate as a subset of NPY$^+$ cells that undergo marked growth during the vocal learning period and are also present in other pallial vocal nuclei (Figures S4I and S4J), and thus may be a fundamental feature shared by songbird vocal learning circuits. The smaller PSPs of the larger GABAergic cells compared to the smaller cells (Figure 4B) suggests that excitatory input to small cells may have a larger impact on spiking probability, as also observed in human cortex GABAergic interneurons.[101]

Mammalian neocortical GABAergic interneurons can be classified into parvalbumin (PVALB; Basket and Chandelier cells), somatostatin (SST; Martinotti and non-Martinotti cells), and ionotropic serotonin receptor (5HT3aR; VIP and non-VIP) interneurons.[102] While PVALB and SST labeled respectively Inhib_1 and Inhib_2, we show that a large proportion of PVALB$^+$ cells in RA are excitatory (Figures S4G and S4H), providing a cellular context for a unique feature of pallial vocal nuclei. Notably, PVALB is also a selective marker of Betz cells among layer 5 pyramidal neurons of human and macaque motor cortex,[103] strengthening our recently described similarity between RAPNs and primate Betz cells.[16] The few VIP-labeled neurons per se did not define an inhibitory cell type, although they may be a subtype of PVALB$^+$ Inhib_1 cells. NPY$^+$ cells (Inhib_2) inside RA included both large and small soma subtypes (Figure 3G), and both display striking rebound spikes after a hyperpolarizing pulse (Figure 4B). Interestingly, this is a hallmark of large cortical Martinotti cells.[104] Neocortical interneurons are also often connected by gap junctions that stabilize circuits and promote oscillations, and likewise GABAergic neurons in RA have extensive expression of the connexin-36 gene, GJD2.[105]

Inhibition plays a critical role in HVC, which exhibits sparse firing,[10,104,106] whereas RA fires continuously at 30–40 Hz and thus may require fewer interneurons, as we find here. However, during singing RA exhibits burst-pause firing driven by HVC inputs to RAPN and perhaps directly to RA interneurons. In this context, the large postsynaptic potentials we show in the GABAergic interneurons could reflect strong synapses from HVC or from RAPN-to-RA-interneuron connections, and they may produce fast and strong inhibitory inputs onto RAPNs, which may be required for rapid pauses in RAPN firing.[10,59,68] The sparse population of GABAergic interneurons in RA contrasts with their higher abundance in other telencephalic areas such as auditory field L2 or the caudomedial nidopallium, where abundant GABAergic synaptic currents can be recorded.[107] Tonic inhibition and a balanced excitation/inhibition ratio are critical to stabilizing microcircuits against runaway excitation. Interestingly, RAPNs do not appear to be highly interconnected,[68] so they may be less prone to runaway excitation. In agreement with our findings, *in vivo* RA recordings reveal rather few single units from interneurons.[108] This reduced number of interneurons may represent a specialized feature of cortical vocal microcircuits, although the large size and unique properties of some inhibitory subtypes may compensate for the sparsity of GABAergic cells in RA.

With exceptions like radial glia in the context of adult neurogenesis[109,110] or the astrocytic expression of aromatase in response to brain injury,[111] non-neuronal cells in the songbird brain have been largely understudied. Our extensive expression profiles and spatial distribution data of non-neuronal AI cell classes include an astrocyte specific to RA. Astrocytes have known roles that impact synaptic function, suggesting that an astrocytic specialization in RA may impact local transmission[112] and potentially impact vocal production. Another striking feature is the large proportion of astrocytes among total RA cells (Figure 1G). Given that RAPNs spontaneously fire spikes at high rates (30–40 Hz) except during their song burst-pause mode, these neurons will be releasing large concentrations of potassium ions to the extracellular space. An abundance of astrocytes, with their high density of Kir4.1 (KCNJ10) inward rectifying potassium channels, will thus be needed to mop up these extracellular ions and maintain cellular ionic gradient homeostasis.[113]

Like in mammals, oligodendrocytes are most commonly found in fiber tracts of the zebra finch brain.[22] Highly myelinated axons allow faster spike propagation and less jitter in spike timing to downstream neurons.[114] The oligodendrocyte enrichment we observed within RA and other pallial song nuclei compared to their surrounds suggests that some local projections intrinsic to these nuclei are myelinated. Surprisingly, oligodendrocyte markers increased in both males and females during development. There is evidence that females retain some song nuclei connectivity,[115] even though they do not sing and their RA shows marked developmental regressions in volume as well as neuronal size and number.[50,52] Our findings suggest that RA connections may be myelinated in females, possibly subserving functions unrelated to singing. Also noteworthy is the male-specific developmental increase in markers of endothelial cells, suggesting a possible expansion of the capillary bed to meet the high metabolic demands of RA.[15,76]

RA has been hypothesized to have evolved in songbirds as a vocal specialization of a more primordial motor-subserving AId previously present in a non-vocal learning avian ancestor (Figure 7G).[25] We recently supported this hypothesis by showing that RA and AId share molecular specializations compared to the rest of the arcopallium,[23] but we now provide a cellular context for those specializations. In a recently proposed duplication and specialization model of cerebellar evolution,[116] when a cerebellar nucleus is duplicated the excitatory neurons diverge in their gene expression and projection targets, while inhibitory neurons are conserved. By analogy, and based on the hypothesis that RA evolved as a specialization of AId,[23,25] RA's excitatory cells have connections distinct from those of the rest of the AI and are molecularly divergent from other AI excitatory cell types. RA's excitatory neurons may thus have evolved through differentiation of an ancestral AI excitatory neuron, adapting expression profiles to enable vocal production via its projections. In comparison, inhibitory neurons are more molecularly conserved throughout the AI, with Inhib_2–4 uniformly distributed, noting, however, that Inhib_1 is largely absent from RA whereas large Inhib_2 cells and an astrocyte subtype are unique to RA.

In sum, by characterizing molecularly defined cell types in RA and other AI subdivisions, our study has identified cellular features that are characteristic of a key vocal-motor cortical nucleus in adult male zebra finches, distinguishing them from those in more general somatic motor and sensory circuits. We present evidence that these features, including RA-unique cell types and lack of some cell types present in other parts of the AI, emerge developmentally during the vocal learning period. We hypothesize that cellular specializations of RA may have originated in evolution from the differentiation of primordial cell types present in an ancestral AI. Our extensive dataset of molecular features of RA cell types provides a rich basis for mechanistic studies aimed at understanding the roles of specific genes in the context of vocal control circuits. Lastly, our data visualization applications allow for easy integration of molecular cellular profiling and developmental transcriptomics with spatial distribution data in the finch arcopallium. Besides facilitating exploration of these rich datasets in songbirds, these resources point to approaches that could be broadly applied to understanding circuits that underlie complex learned behaviors and fine motor control.

Limitations of the study

While the snRNA-seq and bioinformatics analyses suggest specialized roles for a large set of differentially expressed genes and pathways in the identified cell types, the data do not establish direct causal links to the regulation of RA physiology or singing behavior. Mechanistic manipulations of gene expression and/or molecular functions are needed to establish causal links, including those between several recorded electrophysiological features and ion channel gene specializations of RA cell types. We also did not use retrograde tracing to directly assess possible transcriptome differences among neurons that project to vocal and/or respiratory brainstem centers. Our single identified RAPN cluster might thus be non-homogeneous with regard to projection targets, and the lack of regional molecular divergence among RA domains should be taken with caution.

STAR+METHODS

Detailed methods are provided in the online version of this paper and include the following:

SUPPLEMENTAL INFORMATION

Supplemental information can be found online at https://doi.org/10.1016/j.celrep.2023.113344.

ACKNOWLEDGMENTS

We would like to thank Peter Lovell and Leonardo Tavares for assistance with ZEBrA. We would also like to thank the Integrative Genomics Core at OHSU including Robert Searles and Christina Harrington. Funding for this project includes support from T32AG055378 (pre-doctoral) to A.A.N.; NSF IOS 2154646 to H.v.G. and C.V.M.; NIH grants R01DC004274 to H.v.G. and R21OD028774, R03NS115145, and R24GM120464 to C.V.M.; and OHSU's Core Pilot Funds to C.V.M. to support the use of OHSU's Integrated Genomics Laboratory.

AUTHOR CONTRIBUTIONS

A.A.N. performed all molecular experiments with input from C.V.M. B.M.Z. performed all electrophysiology experiments with input from A.A.N. and H.v.G. A.A.N. and B.M.Z. analyzed data. A.A.N. and S.R.F. developed the interactive applications. A.A.N. and C.V.M. wrote the manuscript with input on molecular aspects from S.R.F. and input on electrophysiology aspects written by B.M.Z. and H.v.G.

DECLARATION OF INTERESTS

The authors declare no competing interests.

INCLUSION AND DIVERSITY

We support inclusive, diverse, and equitable conduct of research.

Received: May 22, 2023
Revised: August 30, 2023
Accepted: October 10, 2023

REFERENCES

1. Arendt, D., Musser, J.M., Baker, C.V.H., Bergman, A., Cepko, C., Erwin, D.H., Pavlicev, M., Schlosser, G., Widder, S., Laubichler, M.D., and Wagner, G.P. (2016). The origin and evolution of cell types. Nat. Rev. Genet. *17*, 744–757. https://doi.org/10.1038/nrg.2016.127.
2. Arendt, D. (2008). The evolution of cell types in animals: emerging principles from molecular studies. Nat. Rev. Genet. *9*, 868–882. https://doi.org/10.1038/nrg2416.

3. Jarvis, E.D. (2019). Evolution of vocal learning and spoken language. Science *366*, 50–54. https://doi.org/10.1126/science.aax0287.

4. Karten, H.J. (2013). Neocortical evolution: neuronal circuits arise independently of lamination. Curr. Biol. *23*, R12–R15. https://doi.org/10.1016/j.cub.2012.11.013.

5. Stacho, M., Herold, C., Rook, N., Wagner, H., Axer, M., Amunts, K., and Güntürkün, O. (2020). A cortex-like canonical circuit in the avian forebrain. Science *369*, eabc5534. https://doi.org/10.1126/science.abc5534.

6. Simonyan, K. (2014). The laryngeal motor cortex: its organization and connectivity. Curr. Opin. Neurobiol. *28*, 15–21. https://doi.org/10.1016/j.conb.2014.05.006.

7. Vicario, D.S. (1991). Organization of the zebra finch song control system: II. Functional organization of outputs from nucleus Robustus archistriatalis. J. Comp. Neurol. *309*, 486–494. https://doi.org/10.1002/cne.903090405.

8. Wild, J.M. (1993). Descending projections of the songbird nucleus robustus archistriatalis. J. Comp. Neurol. *338*, 225–241. https://doi.org/10.1002/cne.903380207.

9. Nottebohm, F., Stokes, T.M., and Leonard, C.M. (1976). Central control of song in the canary, Serinus canarius. J. Comp. Neurol. *165*, 457–486. https://doi.org/10.1002/cne.901650405.

10. Hahnloser, R.H.R., Kozhevnikov, A.A., and Fee, M.S. (2002). An ultra-sparse code underlies the generation of neural sequences in a songbird. Nature *419*, 65–70. https://doi.org/10.1038/nature00974.

11. Yu, A.C., and Margoliash, D. (1996). Temporal hierarchical control of singing in birds. Science *273*, 1871–1875. https://doi.org/10.1126/science.273.5283.1871.

12. Sober, S.J., Wohlgemuth, M.J., and Brainard, M.S. (2008). Central contributions to acoustic variation in birdsong. J. Neurosci. *28*, 10370–10379. https://doi.org/10.1523/JNEUROSCI.2448-08.2008.

13. Lemon, R., and Kraskov, A. (2019). Starting and stopping movement by the primate brain. Brain Neurosci. Adv. *3*, 2398212819837149. https://doi.org/10.1177/2398212819837149.

14. Ölveczky, B.P., Otchy, T.M., Goldberg, J.H., Aronov, D., and Fee, M.S. (2011). Changes in the neural control of a complex motor sequence during learning. J. Neurophysiol. *106*, 386–397. https://doi.org/10.1152/jn.00018.2011.

15. Zemel, B.M., Nevue, A.A., Dagostin, A., Lovell, P.V., Mello, C.V., and von Gersdorff, H. (2021). Resurgent Na(+) currents promote ultrafast spiking in projection neurons that drive fine motor control. Nat. Commun. *12*, 6762. https://doi.org/10.1038/s41467-021-26521-3.

16. Zemel, B.M., Nevue, A.A., Tavares, L.E.S., Dagostin, A., Lovell, P.V., Jin, D.Z., Mello, C.V., and von Gersdorff, H. (2023). Motor cortex analogue neurons in songbirds utilize Kv3 subunits to generate ultranarrow spikes. Elife *12*, e81992. https://doi.org/10.7554/eLife.81992.

17. Lemon, R.N., Baker, S.N., and Kraskov, A. (2021). Classification of Cortical Neurons by Spike Shape and the Identification of Pyramidal Neurons. Cerebr. Cortex *31*, 5131–5138. https://doi.org/10.1093/cercor/bhab147.

18. Kittelberger, J.M., and Mooney, R. (1999). Lesions of an avian forebrain nucleus that disrupt song development alter synaptic connectivity and transmission in the vocal premotor pathway. J. Neurosci. *19*, 9385–9398. https://doi.org/10.1523/JNEUROSCI.19-21-09385.1999.

19. Pfenning, A.R., Hara, E., Whitney, O., Rivas, M.V., Wang, R., Roulhac, P.L., Howard, J.T., Wirthlin, M., Lovell, P.V., Ganapathy, G., et al. (2014). Convergent transcriptional specializations in the brains of humans and song-learning birds. Science *346*, 1256846. https://doi.org/10.1126/science.1256846.

20. Lovell, P.V., Huizinga, N.A., Friedrich, S.R., Wirthlin, M., and Mello, C.V. (2018). The constitutive differential transcriptome of a brain circuit for vocal learning. BMC Genom. *19*, 231. https://doi.org/10.1186/s12864-018-4578-0.

21. Mello, C.V., Kaser, T., Buckner, A.A., Wirthlin, M., and Lovell, P.V. (2019). Molecular architecture of the zebra finch arcopallium. J. Comp. Neurol. *527*, 2512–2556. https://doi.org/10.1002/cne.24688.

22. Lovell, P.V., Wirthlin, M., Kaser, T., Buckner, A.A., Carleton, J.B., Snider, B.R., McHugh, A.K., Tolpygo, A., Mitra, P.P., and Mello, C.V. (2020). ZEBrA: Zebra finch Expression Brain Atlas-A resource for comparative molecular neuroanatomy and brain evolution studies. J. Comp. Neurol. *528*, 2099–2131. https://doi.org/10.1002/cne.24879.

23. Nevue, A.A., Lovell, P.V., Wirthlin, M., and Mello, C.V. (2020). Molecular specializations of deep cortical layer analogs in songbirds. Sci. Rep. *10*, 18767. https://doi.org/10.1038/s41598-020-75773-4.

24. Colquitt, B.M., Merullo, D.P., Konopka, G., Roberts, T.F., and Brainard, M.S. (2021). Cellular transcriptomics reveals evolutionary identities of songbird vocal circuits. Science *371*, eabd9704. https://doi.org/10.1126/science.abd9704.

25. Feenders, G., Liedvogel, M., Rivas, M., Zapka, M., Horita, H., Hara, E., Wada, K., Mouritsen, H., and Jarvis, E.D. (2008). Molecular mapping of movement-associated areas in the avian brain: a motor theory for vocal learning origin. PLoS One *3*, e1768. https://doi.org/10.1371/journal.pone.0001768.

26. Zeier, H.J., and Karten, H.J. (1973). Connections of the anterior commissure in the pigeon (Columba livia). J. Comp. Neurol. *150*, 201–216. https://doi.org/10.1002/cne.901500207.

27. Dugas-Ford, J., Rowell, J.J., and Ragsdale, C.W. (2012). Cell-type homologies and the origins of the neocortex. Proc. Natl. Acad. Sci. USA *109*, 16974–16979. https://doi.org/10.1073/pnas.1204773109.

28. Yuan, R.C., and Bottjer, S.W. (2020). Multidimensional Tuning in Motor Cortical Neurons during Active Behavior. eNeuro *7*, ENEURO.0109, 20.2020. https://doi.org/10.1523/ENEURO.0109-20.2020.

29. Mandelblat-Cerf, Y., Las, L., Denisenko, N., and Fee, M.S. (2014). A role for descending auditory cortical projections in songbird vocal learning. Elife *3*, e02152. https://doi.org/10.7554/eLife.02152.

30. Mello, C.V., and Clayton, D.F. (1994). Song-induced ZENK gene expression in auditory pathways of songbird brain and its relation to the song control system. J. Neurosci. *14*, 6652–6666. https://doi.org/10.1523/JNEUROSCI.14-11-06652.1994.

31. Kearney, M.G., Warren, T.L., Hisey, E., Qi, J., and Mooney, R. (2019). Discrete Evaluative and Premotor Circuits Enable Vocal Learning in Songbirds. Neuron *104*, 559–575.e6. https://doi.org/10.1016/j.neuron.2019.07.025.

32. Friedrich, S.R., Nevue, A.A., Andrade, A.L.P., Velho, T.A.F., and Mello, C.V. (2022). Emergence of sex-specific transcriptomes in a sexually dimorphic brain nucleus. Cell Rep. *40*, 111152. https://doi.org/10.1016/j.celrep.2022.111152.

33. Fernández, M., Morales, C., Durán, E., Fernández-Colleman, S., Sentis, E., Mpodozis, J., Karten, H.J., and Marín, G.J. (2020). Parallel organization of the avian sensorimotor arcopallium: Tectofugal visual pathway in the pigeon (Columba livia). J. Comp. Neurol. *528*, 597–623. https://doi.org/10.1002/cne.24775.

34. Zheng, G.X.Y., Terry, J.M., Belgrader, P., Ryvkin, P., Bent, Z.W., Wilson, R., Ziraldo, S.B., Wheeler, T.D., McDermott, G.P., Zhu, J., et al. (2017). Massively parallel digital transcriptional profiling of single cells. Nat. Commun. *8*, 14049. https://doi.org/10.1038/ncomms14049.

35. Zhang, Y., Chen, K., Sloan, S.A., Bennett, M.L., Scholze, A.R., O'Keeffe, S., Phatnani, H.P., Guarnieri, P., Caneda, C., Ruderisch, N., et al. (2014). An RNA-sequencing transcriptome and splicing database of glia, neurons, and vascular cells of the cerebral cortex. J. Neurosci. *34*, 11929–11947. https://doi.org/10.1523/JNEUROSCI.1860-14.2014.

36. Tasic, B., Menon, V., Nguyen, T.N., Kim, T.K., Jarsky, T., Yao, Z., Levi, B., Gray, L.T., Sorensen, S.A., Dolbeare, T., et al. (2016). Adult mouse cortical cell taxonomy revealed by single cell transcriptomics. Nat. Neurosci. *19*, 335–346. https://doi.org/10.1038/nn.4216.

37. von Bartheld, C.S., Bahney, J., and Herculano-Houzel, S. (2016). The search for true numbers of neurons and glial cells in the human brain: A review of 150 years of cell counting. J. Comp. Neurol. *524*, 3865–3895. https://doi.org/10.1002/cne.24040.

38. Bottjer, S.W., Brady, J.D., and Cribbs, B. (2000). Connections of a motor cortical region in zebra finches: relation to pathways for vocal learning. J. Comp. Neurol. *420*, 244–260.

39. Lodato, S., and Arlotta, P. (2015). Generating neuronal diversity in the mammalian cerebral cortex. Annu. Rev. Cell Dev. Biol. *31*, 699–720. https://doi.org/10.1146/annurev-cellbio-100814-125353.

40. Nottebohm, F., and Arnold, A.P. (1976). Sexual dimorphism in vocal control areas of the songbird brain. Science *194*, 211–213. https://doi.org/10.1126/science.959852.

41. Gurney, M.E., and Konishi, M. (1980). Hormone-induced sexual differentiation of brain and behavior in zebra finches. Science *208*, 1380–1383. https://doi.org/10.1126/science.208.4450.1380.

42. Grisham, W., Tam, A., Greco, C.M., Schlinger, B.A., and Arnold, A.P. (1997). A putative 5 alpha-reductase inhibitor demasculinizes portions of the zebra finch song system. Brain Res. *750*, 122–128. https://doi.org/10.1016/s0006-8993(96)01336-4.

43. Rosso, S.B., and Inestrosa, N.C. (2013). WNT signaling in neuronal maturation and synaptogenesis. Front. Cell. Neurosci. *7*, 103. https://doi.org/10.3389/fncel.2013.00103.

44. Song, S.J., Mao, X.G., Wang, C., Han, A.G., Yan, M., and Xue, X.Y. (2015). LGR5/GPR49 is implicated in motor neuron specification in nervous system. Neurosci. Lett. *584*, 135–140. https://doi.org/10.1016/j.neulet.2014.09.056.

45. Carmon, K.S., Gong, X., Lin, Q., Thomas, A., and Liu, Q. (2011). R-spondins function as ligands of the orphan receptors LGR4 and LGR5 to regulate Wnt/beta-catenin signaling. Proc. Natl. Acad. Sci. USA *108*, 11452–11457. https://doi.org/10.1073/pnas.1106083108.

46. McLeod, F., and Salinas, P.C. (2018). Wnt proteins as modulators of synaptic plasticity. Curr. Opin. Neurobiol. *53*, 90–95. https://doi.org/10.1016/j.conb.2018.06.003.

47. Kubikova, L., Wada, K., and Jarvis, E.D. (2010). Dopamine receptors in a songbird brain. J. Comp. Neurol. *518*, 741–769. https://doi.org/10.1002/cne.22255.

48. Liao, C., Wang, S., Pan, X., Hou, G., and Li, D. (2013). Dopamine modulates the excitability of projection neurons in the robust nucleus of the arcopallium in adult zebra finches. PLoS One*8*, e82497. https://doi.org/10.1371/journal.pone.0082497.

49. Dityatev, A., Schachner, M., and Sonderegger, P. (2010). The dual role of the extracellular matrix in synaptic plasticity and homeostasis. Nat. Rev. Neurosci. *11*, 735–746. https://doi.org/10.1038/nrn2898.

50. Nixdorf-Bergweiler, B.E. (1996). Divergent and parallel development in volume sizes of telencephalic song nuclei in male and female zebra finches. J. Comp. Neurol. *375*, 445–456. https://doi.org/10.1002/(SICI)1096-9861(19961118)375:3<445::AID-CNE7>3.0.CO;2-2.

51. Olson, C.R., Hodges, L.K., and Mello, C.V. (2015). Dynamic gene expression in the song system of zebra finches during the song learning period. Dev. Neurobiol. *75*, 1315–1338. https://doi.org/10.1002/dneu.22286.

52. Konishi, M., and Akutagawa, E. (1985). Neuronal growth, atrophy and death in a sexually dimorphic song nucleus in the zebra finch brain. Nature *315*, 145–147. https://doi.org/10.1038/315145a0.

53. Gurney, M.E. (1981). Hormonal control of cell form and number in the zebra finch song system. J. Neurosci. *1*, 658–673. https://doi.org/10.1523/JNEUROSCI.01-06-00658.

54. Arnold, A.P. (1980). Quantitative analysis of sex differences in hormone accumulation in the zebra finch brain: methodological and theoretical issues. J. Comp. Neurol.*189*, 421–436. https://doi.org/10.1002/cne.901890302.

55. Grisham, W., and Arnold, A.P. (1995). A direct comparison of the masculinizing effects of testosterone, androstenedione, estrogen, and progesterone on the development of the zebra finch song system. J. Neurobiol. *26*, 163–170. https://doi.org/10.1002/neu.480260202.

56. Kim, Y.H., Perlman, W.R., and Arnold, A.P. (2004). Expression of androgen receptor mRNA in zebra finch song system: developmental regulation by estrogen. J. Comp. Neurol. *469*, 535–547. https://doi.org/10.1002/cne.11033.

57. Holzenberger, M., Jarvis, E.D., Chong, C., Grossman, M., Nottebohm, F., and Scharff, C. (1997). Selective expression of insulin-like growth factor II in the songbird brain. J. Neurosci. *17*, 6974–6987.

58. Roberts, T.F., Klein, M.E., Kubke, M.F., Wild, J.M., and Mooney, R. (2008). Telencephalic neurons monosynaptically link brainstem and forebrain premotor networks necessary for song. J. Neurosci. *28*, 3479–3489. https://doi.org/10.1523/JNEUROSCI.0177-08.2008.

59. Vicario, D.S., and Raksin, J.N. (2000). Possible roles for GABAergic inhibition in the vocal control system of the zebra finch. Neuroreport *11*, 3631–3635. https://doi.org/10.1097/00001756-200011090-00046.

60. Lim, L., Mi, D., Llorca, A., and Marı´n, O. (2018). Development and Functional Diversification of Cortical Interneurons. Neuron *100*, 294–313. https://doi.org/10.1016/j.neuron.2018.10.009.

61. Bakken, T.E., Jorstad, N.L., Hu, Q., Lake, B.B., Tian, W., Kalmbach, B.E., Crow, M., Hodge, R.D., Krienen, F.M., Sorensen, S.A., et al. (2021). Comparative cellular analysis of motor cortex in human, marmoset and mouse. Nature *598*, 111–119. https://doi.org/10.1038/s41586-021-03465-8.

62. Lein, E.S., Hawrylycz, M.J., Ao, N., Ayres, M., Bensinger, A., Bernard, A., Boe, A.F., Boguski, M.S., Brockway, K.S., Byrnes, E.J., et al. (2007). Genome-wide atlas of gene expression in the adult mouse brain. Nature *445*, 168–176. https://doi.org/10.1038/nature05453.

63. Balmer, T.S., Carels, V.M., Frisch, J.L., and Nick, T.A. (2009). Modulation of perineuronal nets and parvalbumin with developmental song learning. J. Neurosci. *29*, 12878–12885. https://doi.org/10.1523/JNEUROSCI.2974-09.2009.

64. Wild, J.M., Williams, M.N., and Suthers, R.A. (2001). Parvalbumin-positive projection neurons characterise the vocal premotor pathway in male, but not female, zebra finches. Brain Res. *917*, 235–252. https://doi.org/10.1016/s0006-8993(01)02938-9.

65. Hara, E., Rivas, M.V., Ward, J.M., Okanoya, K., and Jarvis, E.D. (2012). Convergent differential regulation of parvalbumin in the brains of vocal learners. PLoS One *7*, e29457. https://doi.org/10.1371/journal.pone.0029457.

66. Pinaud, R., and Mello, C.V. (2007). GABA immunoreactivity in auditory and song control brain areas of zebra finches. J. Chem. Neuroanat. *34*, 1–21. https://doi.org/10.1016/j.jchemneu.2007.03.005.

67. Spiro, J.E., Dalva, M.B., and Mooney, R. (1999). Long-range inhibition within the zebra finch song nucleus RA can coordinate the firing of multiple projection neurons. J. Neurophysiol. *81*, 3007–3020. https://doi.org/10.1152/jn.1999.81.6.3007.

68. Miller, M.N., Cheung, C.Y.J., and Brainard, M.S. (2017). Vocal learning promotes patterned inhibitory connectivity. Nat. Commun. *8*, 2105. https://doi.org/10.1038/s41467-017-01914-5.

69. Dimidschstein, J., Chen, Q., Tremblay, R., Rogers, S.L., Saldi, G.A., Guo, L., Xu, Q., Liu, R., Lu, C., Chu, J., et al. (2016). A viral strategy for targeting and manipulating interneurons across vertebrate species. Nat. Neurosci. *19*, 1743–1749. https://doi.org/10.1038/nn.4430.

70. Liao, S.Q., Hou, G.Q., Liu, X.L., Long, C., and Li, D.F. (2011). Electrophysiological properties of neurons in the robust nucleus of the arcopallium of adult male zebra finches. Neurosci. Lett. *487*, 234–239. https://doi.org/10.1016/j.neulet.2010.10.029.

71. Jerng, H.H., Shahidullah, M., and Covarrubias, M. (1999). Inactivation gating of Kv4 potassium channels: molecular interactions involving the inner vestibule of the pore. J. Gen. Physiol. *113*, 641–660. https://doi.org/10.1085/jgp.113.5.641.

72. Blaine, J.T., and Ribera, A.B. (2001). Kv2 channels form delayed-rectifier potassium channels in situ. J. Neurosci. *21*, 1473–1480. https://doi.org/10.1523/JNEUROSCI.21-05-01473.2001.

73. Bond, C.T., Maylie, J., and Adelman, J.P. (2005). SK channels in excitability, pacemaking and synaptic integration. Curr. Opin. Neurobiol. *15*, 305–311. https://doi.org/10.1016/j.conb.2005.05.001.

74. Champoux, K.L., Miller, K.E., and Perkel, D.J. (2021). Differential development of myelin in zebra finch song nuclei. J. Comp. Neurol. *529*, 1255–1265. https://doi.org/10.1002/cne.25019.

75. Karten, H.J., Brzozowska-Prechtl, A., Lovell, P.V., Tang, D.D., Mello, C.V., Wang, H., and Mitra, P.P. (2013). Digital atlas of the zebra finch (Taeniopygia guttata) brain: a high-resolution photo atlas. J. Comp. Neurol. *521*, 3702–3715. https://doi.org/10.1002/cne.23443.

76. Adret, P., and Margoliash, D. (2002). Metabolic and neural activity in the song system nucleus robustus archistriatalis: effect of age and gender. J. Comp. Neurol. *454*, 409–423. https://doi.org/10.1002/cne.10459.

77. Ball, G.F., Nock, B., Wingfield, J.C., McEwen, B.S., and Balthazart, J. (1990). Muscarinic cholinergic receptors in the songbird and quail brain: a quantitative autoradiographic study. J. Comp. Neurol. *298*, 431–442. https://doi.org/10.1002/cne.902980405.

78. Wood, W.E., Lovell, P.V., Mello, C.V., and Perkel, D.J. (2011). Serotonin, via HTR2 receptors, excites neurons in a cortical-like premotor nucleus necessary for song learning and production. J. Neurosci. *31*, 13808–13815. https://doi.org/10.1523/JNEUROSCI.2281-11.2011.

79. Kubíková, L., Výboh, P., and Kostál, L. (2009). Kinetics and pharmacology of the D1- and D2-like dopamine receptors in Japanese quail brain. Cell. Mol. Neurobiol. *29*, 961–970. https://doi.org/10.1007/s10571-009-9382-6.

80. Asogwa, N.C., Mori, C., Sánchez-Valpuesta, M., Hayase, S., and Wada, K. (2018). Inter- and intra-specific differences in muscarinic acetylcholine receptor expression in the neural pathways for vocal learning in songbirds. J. Comp. Neurol. *526*, 2856–2869. https://doi.org/10.1002/cne.24532.

81. Shea, S.D., Koch, H., Baleckaitis, D., Ramirez, J.M., and Margoliash, D. (2010). Neuron-specific cholinergic modulation of a forebrain song control nucleus. J. Neurophysiol. *103*, 733–745. https://doi.org/10.1152/jn.00803.2009.

82. Wood, W.E., Roseberry, T.K., and Perkel, D.J. (2013). HTR2 receptors in a songbird premotor cortical-like area modulate spectral characteristics of zebra finch song. J. Neurosci. *33*, 2908–2915. https://doi.org/10.1523/JNEUROSCI.4291-12.2013.

83. Meng, W., Wang, S., Yao, L., Zhang, N., and Li, D. (2017). Muscarinic Receptors Are Responsible for the Cholinergic Modulation of Projection Neurons in the Song Production Brain Nucleus RA of Zebra Finches. Front. Cell. Neurosci. *11*, 51. https://doi.org/10.3389/fncel.2017.00051.

84. Wang, S., Liu, S., Wang, Q., Sun, Y., Yao, L., Li, D., and Meng, W. (2020). Dopamine Modulates Excitatory Synaptic Transmission by Activating Presynaptic D1-like Dopamine Receptors in the RA Projection Neurons of Zebra Finches. Front. Cell. Neurosci. *14*, 126. https://doi.org/10.3389/fncel.2020.00126.

85. Balthazart, J., Voigt, C., Boseret, G., and Ball, G.F. (2008). Expression of reelin, its receptors and its intracellular signaling protein, Disabled1 in the canary brain: relationships with the song control system. Neuroscience *153*, 944–962. https://doi.org/10.1016/j.neuroscience.2008.02.020.

86. Mendoza, E., Tokarev, K., Düring, D.N., Retamosa, E.C., Weiss, M., Arpenik, N., and Scharff, C. (2015). Differential coexpression of FoxP1, FoxP2, and FoxP4 in the Zebra Finch (Taeniopygia guttata) song system. J. Comp. Neurol. *523*, 1318–1340. https://doi.org/10.1002/cne.23731.

87. Pramod, A.B., Foster, J., Carvelli, L., and Henry, L.K. (2013). SLC6 transporters: structure, function, regulation, disease association and therapeutics. Mol. Aspect. Med. *34*, 197–219. https://doi.org/10.1016/j.mam.2012.07.002.

88. Harik, S.I., Kalaria, R.N., Andersson, L., Lundahl, P., and Perry, G. (1990). Immunocytochemical localization of the erythroid glucose transporter: abundance in tissues with barrier functions. J. Neurosci. *10*, 3862–3872. https://doi.org/10.1523/JNEUROSCI.10-12-03862.1990.

89. Zeier, H., and Karten, H.J. (1971). The archistriatum of the pigeon: organization of afferent and efferent connections. Brain Res. *31*, 313–326. https://doi.org/10.1016/0006-8993(71)90185-5.

90. Moses, L., and Pachter, L. (2022). Museum of spatial transcriptomics. Nat. Methods *19*, 534–546. https://doi.org/10.1038/s41592-022-01409-2.

91. Friedrich, S.R., Lovell, P.V., Kaser, T.M., and Mello, C.V. (2019). Exploring the molecular basis of neuronal excitability in a vocal learner. BMC Genom. *20*, 629. https://doi.org/10.1186/s12864-019-5871-2.

92. Kim, J.H., Kushmerick, C., and von Gersdorff, H. (2010). Presynaptic resurgent Na+ currents sculpt the action potential waveform and increase firing reliability at a CNS nerve terminal. J. Neurosci. *30*, 15479–15490. https://doi.org/10.1523/JNEUROSCI.3982-10.2010.

93. Kodama, T., Gittis, A.H., Shin, M., Kelleher, K., Kolkman, K.E., McElvain, L., Lam, M., and du Lac, S. (2020). Graded Coexpression of Ion Channel, Neurofilament, and Synaptic Genes in Fast-Spiking Vestibular Nucleus Neurons. J. Neurosci. *40*, 496–508. https://doi.org/10.1523/JNEUROSCI.1500-19.2019.

94. Schlinger, B.A., and Arnold, A.P. (1991). Androgen effects on the development of the zebra finch song system. Brain Res. *561*, 99–105. https://doi.org/10.1016/0006-8993(91)90754-j.

95. Harding, C.F., Sheridan, K., and Walters, M.J. (1983). Hormonal specificity and activation of sexual behavior in male zebra finches. Horm. Behav. *17*, 111–133. https://doi.org/10.1016/0018-506x(83)90021-1.

96. Tran, D.Q., Andersson, J., Wang, R., Ramsey, H., Unutmaz, D., and Shevach, E.M. (2009). GARP (LRRC32) is essential for the surface expression of latent TGF-beta on platelets and activated FOXP3+ regulatory T cells. Proc. Natl. Acad. Sci. USA *106*, 13445–13450. https://doi.org/10.1073/pnas.0901944106.

97. Safra, N., Bassuk, A.G., Ferguson, P.J., Aguilar, M., Coulson, R.L., Thomas, N., Hitchens, P.L., Dickinson, P.J., Vernau, K.M., Wolf, Z.T., and Bannasch, D.L. (2013). Genome-wide association mapping in dogs enables identification of the homeobox gene, NKX2-8, as a genetic component of neural tube defects in humans. PLoS Genet. *9*, e1003646. https://doi.org/10.1371/journal.pgen.1003646.

98. Sahni, V., Itoh, Y., Shnider, S.J., and Macklis, J.D. (2021). Crim1 and Kelch-like 14 exert complementary dual-directional developmental control over segmentally specific corticospinal axon projection targeting. Cell Rep. *37*, 109842. https://doi.org/10.1016/j.celrep.2021.109842.

99. Wang, R., Chen, C.C., Hara, E., Rivas, M.V., Roulhac, P.L., Howard, J.T., Chakraborty, M., Audet, J.N., and Jarvis, E.D. (2015). Convergent differential regulation of SLIT-ROBO axon guidance genes in the brains of vocal learners. J. Comp. Neurol. *523*, 892–906. https://doi.org/10.1002/cne.23719.

100. Yuan, R.C., and Bottjer, S.W. (2019). Differential developmental changes in cortical representations of auditory-vocal stimuli in songbirds. J. Neurophysiol. *121*, 530–548. https://doi.org/10.1152/jn.00714.2018.

101. Kim, M.H., Radaelli, C., Thomsen, E.R., Monet, D., Chartrand, T., Jorstad, N.L., Mahoney, J.T., Taormina, M.J., Long, B., Baker, K., et al. (2023). Target cell-specific synaptic dynamics of excitatory to inhibitory neuron connections in supragranular layers of human neocortex. Elife *12*, e81863. https://doi.org/10.7554/eLife.81863.

102. Tremblay, R., Lee, S., and Rudy, B. (2016). GABAergic Interneurons in the Neocortex: From Cellular Properties to Circuits. Neuron *91*, 260–292. https://doi.org/10.1016/j.neuron.2016.06.033.

103. Szocsics, P., Papp, P., Havas, L., Watanabe, M., and Magló́czky, Z. (2021). Perisomatic innervation and neurochemical features of giant pyramidal neurons in both hemispheres of the human primary motor cortex. Brain Struct. Funct. *226*, 281–296. https://doi.org/10.1007/s00429-020-02182-8.

104. Hilscher, M.M., Leão, R.N., Edwards, S.J., Leão, K.E., and Kullander, K. (2017). Chrna2-Martinotti Cells Synchronize Layer 5 Type A Pyramidal

Cells via Rebound Excitation. PLoS Biol. *15*, e2001392. https://doi.org/10.1371/journal.pbio.2001392.

105. Alcami, P., Totagera, S., Sohnius-Wilhelmi, N., Leitner, S., Grothe, B., Frankl-Vilches, C., and Gahr, M. (2021). Extensive GJD2 Expression in the Song Motor Pathway Reveals the Extent of Electrical Synapses in the Songbird Brain. Biology *10*, 1099. https://doi.org/10.3390/biology10111099.

106. Vallentin, D., Kosche, G., Lipkind, D., and Long, M.A. (2016). Neural circuits. Inhibition protects acquired song segments during vocal learning in zebra finches. Science *351*, 267–271. https://doi.org/10.1126/science.aad3023.

107. Pinaud, R., Velho, T.A.F., Jeong, J.K., Tremere, L.A., Leão, R.M., von Gersdorff, H., and Mello, C.V. (2004). GABAergic neurons participate in the brain's response to birdsong auditory stimulation. Eur. J. Neurosci. *20*, 1318–1330. https://doi.org/10.1111/j.1460-9568.2004.03585.x.

108. Leonardo, A., and Fee, M.S. (2005). Ensemble coding of vocal control in birdsong. J. Neurosci. *25*, 652–661. https://doi.org/10.1523/JNEUROSCI.3036-04.2005.

109. Alvarez-Buylla, A., Theelen, M., and Nottebohm, F. (1988). Mapping of radial glia and of a new cell type in adult canary brain. J. Neurosci. *8*, 2707–2712. https://doi.org/10.1523/JNEUROSCI.08-08-02707.1988.

110. Alvarez-Buylla, A., and Nottebohm, F. (1988). Migration of young neurons in adult avian brain. Nature *335*, 353–354. https://doi.org/10.1038/335353a0.

111. Saldanha, C.J. (2021). Glial estradiol synthesis after brain injury. Curr. Opin. Endocr. Metab. Res. *21*, 100298. https://doi.org/10.1016/j.coemr.2021.100298.

112. Santello, M., Toni, N., and Volterra, A. (2019). Astrocyte function from information processing to cognition and cognitive impairment. Nat. Neurosci. *22*, 154–166. https://doi.org/10.1038/s41593-018-0325-8.

113. Beckner, M.E. (2020). A roadmap for potassium buffering/dispersion via the glial network of the CNS. Neurochem. Int. *136*, 104727. https://doi.org/10.1016/j.neuint.2020.104727.

114. Kim, J.H., Renden, R., and von Gersdorff, H. (2013). Dysmyelination of auditory afferent axons increases the jitter of action potential timing during high-frequency firing. J. Neurosci. *33*, 9402–9407. https://doi.org/10.1523/JNEUROSCI.3389-12.2013.

115. Shaughnessy, D.W., Hyson, R.L., Bertram, R., Wu, W., and Johnson, F. (2019). Female zebra finches do not sing yet share neural pathways necessary for singing in males. J. Comp. Neurol. *527*, 843–855. https://doi.org/10.1002/cne.24569.

116. Kebschull, J.M., Richman, E.B., Ringach, N., Friedmann, D., Albarran, E., Kolluru, S.S., Jones, R.C., Allen, W.E., Wang, Y., Cho, S.W., et al. (2020). Cerebellar nuclei evolved by repeatedly duplicating a conserved cell-type set. Science *370*, eabd5059. https://doi.org/10.1126/science.abd5059.

117. Lee, E., Choi, J., Jo, Y., Kim, J.Y., Jang, Y.J., Lee, H.M., Kim, S.Y., Lee, H.J., Cho, K., Jung, N., et al. (2016). ACT-PRESTO: Rapid and consistent tissue clearing and labeling method for 3-dimensional (3D) imaging. Sci. Rep. *6*, 18631. https://doi.org/10.1038/srep18631.

118. Replogle, K., Arnold, A.P., Ball, G.F., Band, M., Bensch, S., Brenowitz, E.A., Dong, S., Drnevich, J., Ferris, M., George, J.M., et al. (2008). The Songbird Neurogenomics (SoNG) Initiative: community-based tools and strategies for study of brain gene function and evolution. BMC Genom. *9*, 131. https://doi.org/10.1186/1471-2164-9-131.

119. Stuart, T., Butler, A., Hoffman, P., Hafemeister, C., Papalexi, E., Mauck, W.M., 3rd, Hao, Y., Stoeckius, M., Smibert, P., and Satija, R. (2019). Comprehensive Integration of Single-Cell Data. Cell *177*, 1888–1902.e21. https://doi.org/10.1016/j.cell.2019.05.031.

120. Bolger, A.M., Lohse, M., and Usadel, B. (2014). Trimmomatic: a flexible trimmer for Illumina sequence data. Bioinformatics *30*, 2114–2120. https://doi.org/10.1093/bioinformatics/btu170.

121. Andrews, S. (2010). FastQC: A Quality Control Tool for High Throughput Sequence Data.

122. Dobin, A., Davis, C.A., Schlesinger, F., Drenkow, J., Zaleski, C., Jha, S., Batut, P., Chaisson, M., and Gingeras, T.R. (2013). STAR: ultrafast universal RNA-seq aligner. Bioinformatics *29*, 15–21. https://doi.org/10.1093/bioinformatics/bts635.

123. Love, M.I., Huber, W., and Anders, S. (2014). Moderated estimation of fold change and dispersion for RNA-seq data with DESeq2. Genome Biol. *15*, 550. https://doi.org/10.1186/s13059-014-0550-8.

124. Rhie, A., McCarthy, S.A., Fedrigo, O., Damas, J., Formenti, G., Koren, S., Uliano-Silva, M., Chow, W., Fungtammasan, A., Kim, J., et al. (2021). Towards complete and error-free genome assemblies of all vertebrate species. Nature *592*, 737–746. https://doi.org/10.1038/s41586-021-03451-0.

125. Carleton, J.B., Lovell, P.V., McHugh, A., Marzulla, T., Horback, K.L., and Mello, C.V. (2014). An optimized protocol for high-throughput in situ hybridization of zebra finch brain. Cold Spring Harb. Protoc. *2014*, 1249–1258. https://doi.org/10.1101/pdb.prot084582.

126. Susaki, E.A., Tainaka, K., Perrin, D., Yukinaga, H., Kuno, A., and Ueda, H.R. (2015). Advanced CUBIC protocols for whole-brain and whole-body clearing and imaging. Nat. Protoc. *10*, 1709–1727. https://doi.org/10.1038/nprot.2015.085.

127. Kamburov, A., Wierling, C., Lehrach, H., and Herwig, R. (2009). ConsensusPathDB–a database for integrating human functional interaction networks. Nucleic Acids Res. *37*, D623–D628. https://doi.org/10.1093/nar/gkn698.

STAR+METHODS

KEY RESOURCES TABLE

REAGENT or RESOURCE	SOURCE	IDENTIFIER
Antibodies		
Anti-Digoxigenin-AP, Fab fragments	Roche	Cat# 11093274910; RRID:AB_514497
Anti-Digoxigenin-POD, Fab fragments	Roche	Cat# 11207733910; RRID:AB_514500
Bacterial and virus strains		
pAAV-mDlx-GFP-Fishell-1	Dimidschstein et al.[69]	Addgene Plasmid #83900
Chemicals, peptides, and recombinant proteins		
Platinum Taq DNA Polymerase	Invitrogen	Cat#10966018
2-mercaptoethanol	Sigma-Aldrich	Cat#M3148
DIG RNA Labeling Mix	Roche	Cat#11277073910
Triethanolamine	Fisher	Cat#T350
Formamide	Fisher	Cat#F84
BCIP/NBT	Perkin-Elmer	Cat#NEL937
Acetic Anhydride	Sigma	Cat#A6404
Triton X-100	Sigma	Cat#T8787
BSSHII	NEB	Cat#R0199S
T3 RNA Polymerase	Promega	Cat#P208C
Tyramide conjugates	Invitrogen	Cat#B40952; B40953
CUBIC reagent	Lee et al.[117]	N/A
Critical commercial assays		
Chromium Single Cell 3^{0} Library & Gel Bead Kit v3	10x Genomics	N/A
SmartSeq v4 PLUS kit	Takara Bio USA	Cat#R400752
RNeasy Micro Kit	Qiagen	Cat#74004
Deposited data		
Cell type specializations of the vocal-motor cortex in songbirds	Gene Expression Omnibus (GEO)	GSE233643
Emergence of sex-specific transcriptomes in a sexually-dimorphic brain nucleus	Gene Expression Omnibus (GEO)	GSE191296
ZEBrA interactive applications to examine processed single nuclei and bulk RNAseq datasets	ZEBrA (Zebra Finch Expression Brain Atlas)	www.zebrafinchatlas.org
bTaeGut1_v1.p Taeniopygia guttata assembly	NCBI	GCF_003957565.1
Taeniopygia guttata Annotation Release 104	NCBI	https://www.ncbi.nlm.nih.gov/genome/annotation_euk/Taeniopygia_guttata/104/
Experimental models: Organisms/strains		
Zebra finch (*Taeniopygia guttata*)	Mello lab (OHSU) and Magnolia Bird Farm (Riverside, CA)	N/A
Oligonucleotides		
SRD5A2-Forward: GAGAGGTGGGAGGGTCTCAT	This study	N/A
SRD5A2-Reverse: TCCATGTGTGCAGTGTGGTC	This study	N/A
Recombinant DNA		
ESTIMA collection of zebra finch brain cDNA clones used for riboprobe synthesis for *in situ* hybridizations	Replogle et al.[118]	N/A

(*Continued on next page*)

Continued

REAGENT or RESOURCE	SOURCE	IDENTIFIER
Software and algorithms		
Seurat (v3)	Stuart et al.[119]	https://satijalab.org/seurat/
trimmomatic (v0.36)	Bogler et al.[120]	http://www.usadellab.org/cms/?page=trimmomatic
FastQC (v0.11.9)	Andrews[121]	https://www.bioinformatics.babraham.ac.uk/projects/fastqc/
STAR (v2.6.1)	Dobin et al.[122]	https://github.com/alexdobin/STAR
DESeq2 (v1.30.1)	Love et al.[123]	https://bioconductor.org/packages/release/bioc/html/DESeq2.html
Custom code for generating Shiny Apps	This paper	https://doi.org/10.5281/zenodo.8394120 https://doi.org/10.5281/zenodo.8394118

RESOURCE AVAILABILITY

Lead contact

Further information and requests for resources and reagents should be directed to and will be fulfilled by the lead contact, Claudio V. Mello (melloc@ohsu.edu).

Materials availability

This study did not generate new unique reagents.

Data and code availability

Raw and processed data that were generated and analyzed in this study have been deposited at NCBI's Gene Expression Omnibus (GEO: GSE233643 and GEO: GSE191296) and are publicly available as of the date of publication. Data visualization applications to interact with the single nuclei and bulk RNAseq datasets used in this study were developed using the Shiny R package. The codes used to develop these applications are available at doi.org/10.5281/zenodo.8394120 and doi.org/10.5281/zenodo.8394118. The applications themselves are hosted and deployed using shinyapps.io, and can be accessed for examination and mining of processed data on the homepage of our spatial gene expression atlas ZEBrA at www.zebrafinchatlas.org. Any additional information is available upon request and will be fulfilled by the lead contact Claudio V. Mello (melloc@ohsu.edu).

EXPERIMENTAL MODEL AND SUBJECT DETAILS

All procedures involving live animals were approved by OHSU's IACUC (TR02_IP00000146) and are in accordance with NIH guidelines. Adult male zebra finches (*Taeniopygia guttata*) were isolated in a sound dampening chamber overnight and sacrificed by decapitation the next morning prior to lights on to minimize auditory, vocal, and movement-related activity dependent changes in gene expression. Juvenile zebra finch brains were prepared as previously described.[15,23]

METHOD DETAILS

Single nuclei isolation and sequencing

Frontal slices (400 mm thick, one slice per hemisphere) containing RA, AId, and AIv were cut on a Leica VT1200S vibratome in an ice-cold cutting solution containing 119 mM NaCl, 2.5 mM KCl, 8 mM $MgSO_4$, 16.2 mM $NaHCO_3$, 10 mM HEPES, 1 mM NaH_2PO_4, 0.5 mM $CaCl_2$, 11 mM D-Glucose, 35 mM sucrose with a pH of 7.3–7.4 when bubbled with carbogen (95% O_2, 5% CO_2; 330–340 mOsm). Slices were then transferred to an incubation chamber containing artificial cerebral spinal fluid with 119 mM NaCl, 2.5 mM KCl, 1.3 mM $MgSO_4$, 26.2 mM $NaHCO_3$, 1 mM NaH_2PO_4, 1.5 mM $CaCl_2$, 11 mM D-Glucose, 35 mM sucrose with a pH of 7.3–7.4 when bubbled with carbogen (95% O_2, 5% CO_2; 330–340 mOsm) at 37 C. Microbiopsies containing RA, AId, and AIv were dissected using a scalpel and angled forceps and flash frozen in a dry ice/isopropyl alcohol slurry. Tissue was homogenized in 300 mL of nuclei lysis buffer (10 mM Tris pH 8.0, 250 mM sucrose, 25 mM KCl, 5 mM $MgCl_2$, 0.1% Triton X-100, 0.5% RNasin, and 0.1 mM DTT). 700 mL of lysis buffer was added to the homogenate and the sample was incubated on ice for 5 min. The sample was transferred to a 15 mL conical tube and centrifuged at 500 x g for 5 min at 4C. The supernatant was discarded, 1 mL of ice-cold lysis buffer was added, and the mix was incubated on ice for 5 min. The sample then was centrifuged at 500 x g for 5 min at 4C. The pellet was resuspended in 1 mL of nuclei suspension buffer (1x PBS, 0.01% BSA, and 0.1% RNasin), and filtered through an FLOWMI 40 mm tip strainer (Bel-Art) and centrifuged at 500 x g for 5 min at 4 C. The pelleted nuclei were resuspended in nuclei suspension buffer. Libraries were prepared using the Chromium Single Cell 3^0 Library & Gel Bead Kit v3 (10x Genomics) according to the manufacturer's instructions. Libraries were sequenced using an Illumina NovaSeq 6000 at the Massively Parallel Sequencing Shared Resource at OHSU. Reads were aligned to the zebra finch genome available at Ensembl.org (Taegut1) using CellRanger with include-introns. SnRNA-seq data was processed using a standard Seurat workflow.[119]

Bulk RNA-sequencing

The caudodorsal and rostroventral portions of RA (each an estimated 1/3 area of RA in a slice) were microdissected from a 400 mm thick sagittal vibratome slice (n = 4 animals), prepared as described above for snRNA-seq. The dorsal/ventral axis was defined as orthogonal to the descending occipito-mesencephalic tract (OM), and subregions dissected based on the pattern of retrogradely labeled cells in RA from previous studies.[7,8,58] RNA from these samples were isolated using a Qiagen RNeasy Micro Kit and cDNA libraries were generated using Takara Bio SmartSeq v4 PLUS kit. Paired-end sequencing (2 x 100 bp) was performed on an Illumina NovaSeq 6000 with a target depth of 50M reads per sample. Trimming was performed with trimmomatic (v0.36) and quality control with FastQC (v0.11.9) with no issues detected. STAR (v2.6.1) was used to align sequencing reads and generate read counts per gene using bTaeGut1_v1.p assembly (GCF_003957565.1) and associated genome features from the NCBI annotation release 104 for zebra finch.[124]

In situ hybridization

In situ hybridizations were carried out as previously described.[23,125] All cDNA probes were derived from clones from the ESTIMA collection[118] and had been previously described[32] except for PLP1 (FE722130), RGS10 (CK312091), NPY (CK310313), COLEC12 (DV954836), VWC2 (DV959856), CRISPLD1 (FE712375), CERKL (DV945272), and ADCYAP1 (FE717884). To maximize specificity, we chose clones that aligned to the 3′-untranslated sequence and to a single locus in the zebra finch genome. We cloned the 3′ region of one gene (SRD5A2), for which there was no cDNA clone available, from genomic DNA using PCR (F: GAGAGGTGGGAGGGTCTCAT, R: TCC ATGTGTGCAGTGTGGTC), followed by a second round of PCR with a primer containing the T3 polymerase promoter. Briefly, plasmids containing cDNA of the gene of interest were isolated and restriction enzyme digested with BSSHII to release the insert. The insert was purified using a QIAquick PCR purification kit (Qiagen). Antisense digoxygenin(DIG)-tagged riboprobes were synthesized by *in vitro* transcription using T3 polymerase (Promega) and purified using a Sephadex G-50 column. Probes were hybridized to sections overnight at 65 C followed by a series of high stringency washes. Sections were blocked and incubated in an alkaline phosphatase(AP)-tagged anti-DIG-antibody (1:600; Roche) for 2 h and incubated in BCIP/NBT chromogen (PerkinElmer) overnight. For fluorescent *in situ* hybridizations, following the high stringency washes, sections blocked and incubated in an peroxidase-tagged anti-DIG-antibody (1:600; Roche) for 2 h. Slices were then washed and incubated in Alexa 350 or 488-conjugated tyramide (1:100; Invitrogen) for 2 h. Positive control probes with known expression patterns and no probe negative controls were regularly included in hybridizations.

Electrophysiological characterization of GABAergic neurons

To virally target GABAergic interneurons in the arcopallium, we used AAV9-mDlx-GFP (Addgene #83900)[69]; Stereotaxic injections of 500 nL of AAV were made bilaterally into RA of adult male zebra finches anesthetized with isoflurane. Coordinates used for RA were AP: 0.5mm, ML: 2.2–2.7mm, DV: 2.5mm. Birds were allowed to recover for 2–3 weeks before being sacrificed. Vibratome slices (200 mm) were cut on a vibratome (VT1000, Leica) in an ice-cold cutting solution containing (in mM): 119 NaCl, 2.5 KCl, 8 $MgSO_4$, 16.2 $NaHCO_3$, 10 HEPES, 1 NaH_2PO_4, 0.5 $CaCl_2$, 11 d-Glucose, 35 sucrose, pH 7.3–7.4 that was bubbled with carbogen (95% O_2, 5% CO_2; osmolarity 330–340 mOsm). Slices were then transferred to an incubation chamber containing artificial cerebral spinal fluid (aCSF) with (in mM): 119 NaCl, 2.5 KCl, 1.3 $MgSO_4$, 26.2 $NaHCO_3$, 1 NaH_2PO_4, 1.5 $CaCl_2$, 11 d-Glucose, 35 sucrose, pH 7.3–7.4 when bubbled with carbogen (95% O_2, 5% CO_2; osmolarity 330–340 mOsm) for 10 min at 37 C, followed by a room temperature incubation for 30 min prior to start of electrophysiology experiments.

RA was visualized using differential interference contrast microscopy and transduced cells in RA were visualized using a 488 nm filter. Whole-cell current-clamp recordings were made using a HEKA EPC-10/2 amplifier controlled by Patchmaster software (HEKA, Ludwigshafen/Rhein, Germany). Data were acquired at 100 kHz and low-pass filtered at 2.9 kHz. Patch pipettes were pulled from standard borosilicate capillary glass (WPI, Sarasota, FL, USA) with a P97 puller (Sutter Instruments, Novato, CA). All recording pipettes had a 3.0 to 6.0 MU open-tip resistance in the bath solution. Electrophysiology data were analyzed offline using custom written routines in IGOR Pro (WaveMetrics, Lake Oswego, OR, USA). Intracellular solutions contained (in mM): 142.5 K-Gluconate, 21.9 KCl, 5.5 Na_2-phosphocreatine, 10.9 HEPES, 5.5 EGTA, 4.2 Mg-ATP and 0.545 GTP, pH adjusted to 7.3 with KOH, 330–340 mOsm. To initiate current clamp recordings, we first established a giga-ohm seal in the voltage-clamp configuration, set the pipette capacitance compensation (C-fast), and then set the voltage command to 70 mV. We then applied negative pressure to break into the cell. Once stable, we switched to the current-clamp configuration. Whole-cell current-clamp recordings were performed at room temperature as described in.[15] We note that recordings were not corrected for a liquid junction potential of +9 mV. Capacitance was calculated from the measured membrane time constant, as measured with a single exponential, and input resistance ($t_m = R_{in}, C_m$). Principal component analysis was performed using scikit-learn in a Jupyter Python environment. Inputs to the principal component analysis were the spontaneous number of action potentials, threshold, amplitude, half-width, max depolarization rate, max repolarization rate, peak and afterhyperpolarization, and the number of action potentials, threshold, amplitude, half-width after a 100pA current injection. For the principal component analysis, any missing values were imputed by using the average value of the measurement based on the size classification.

In separate birds, following the 2-week recovery time we perfused the bird with 0.9% saline followed by 3% paraformaldehyde. Brains were dissected and post-fixed in 3% PFA overnight at 4 C before being transferred to PBS. 200 mm thick slices were cut on a vibratome and transferred to a well plate containing CUBIC reagent overnight.[117,126] Slices were then mounted on slides, coverslipped, and imaged on a ZEISS LSM 980 confocal microscope for GFP visualization.

QUANTIFICATION AND STATISTICAL ANALYSIS

snRNA-seq differential gene expression

Clusters were resolved using FindClusters() with a resolution of 0.25 and visualized with a UMAP projection. Differential gene expression was defined using FindMarkers() with min.pct of 0.25. One cluster exhibited differential markers with low percent of cells (<50%) exhibiting the defining marker and with a majority of markers having a negative average logFC, suggesting low quality nuclei and was excluded from further analysis.

Bulk RNA-seq

We also analyzed an existing bulk RNA-seq dataset (GEO: GSE191296).[32] This dataset is comprised of microdissections of RA from 20 dph to 50 dph male and female zebra finches. Count tables were downloaded from the NCBI GEO repository and transcript abundances were plotted using custom code.[32] As described in Friedrich et al.,[32] a binomial generalized linear model was fit to the data with sex and age as main factors with a sex + age interaction. Wald tests were performed on specific contrasts using independent filtering, and genes with a Benjamini-Hochberg-based false discovery rate (FDR) < 0.01 were considered significant.

Gene ontology

To manually curate unannotated Ensembl models among the top 25 markers for the identified clusters, we retrieved the respective sequences from Ensembl.org, BLAST aligned them to zebra finch refseq_rna and refseq_genome databases, and verified the human orthology of the top BLAST hits by further cross-alignments and synteny examination. The complete curated lists of markers for all identified clusters are presented in Table S1, using HUGO terms, except for loci identified as coding long non-coding transcripts (lncs) or still of undefined identify (RefSeq LOC terms). ConsensusPathDB[127] was used for pathway enrichment analysis. All pathways were selected with a minimum overlap of 2 and p value cutoff of 0.05. Protein complex-based gene sets were also selected with the same criteria.

Analysis of in situ hybridization images

Images of *in situ* hybridizations were captured on a Nikon Eclipse E600 microscope, yoked to a PC. Proportion of cell types in each arcopallial subdivision was determined by quantifying an 200 3 200 mm square window in each subdivision, using Neurolucida (Microbrightfield). Cell soma sizes were quantified using ImageJ. Images were converted into 8-bit, thresholded to remove background and subjected to two binary processes (close- and open) to generate particles. For the images from ZEBrA,[22] optical density measurements were taken in ImageJ in RA and HVC as well as the shelf of HVC (ventral to HVC) and the cup of RA (located rostro-ventral to RA). Statistical tests were performed using GraphPad Prism.

Cell Reports, Volume 42

Supplemental information

Cell type specializations

of the vocal-motor cortex in songbirds

Alexander A. Nevue, Benjamin M. Zemel, Samantha R. Friedrich, Henrique von Gersdorff, and Claudio V. Mello

Figure S1

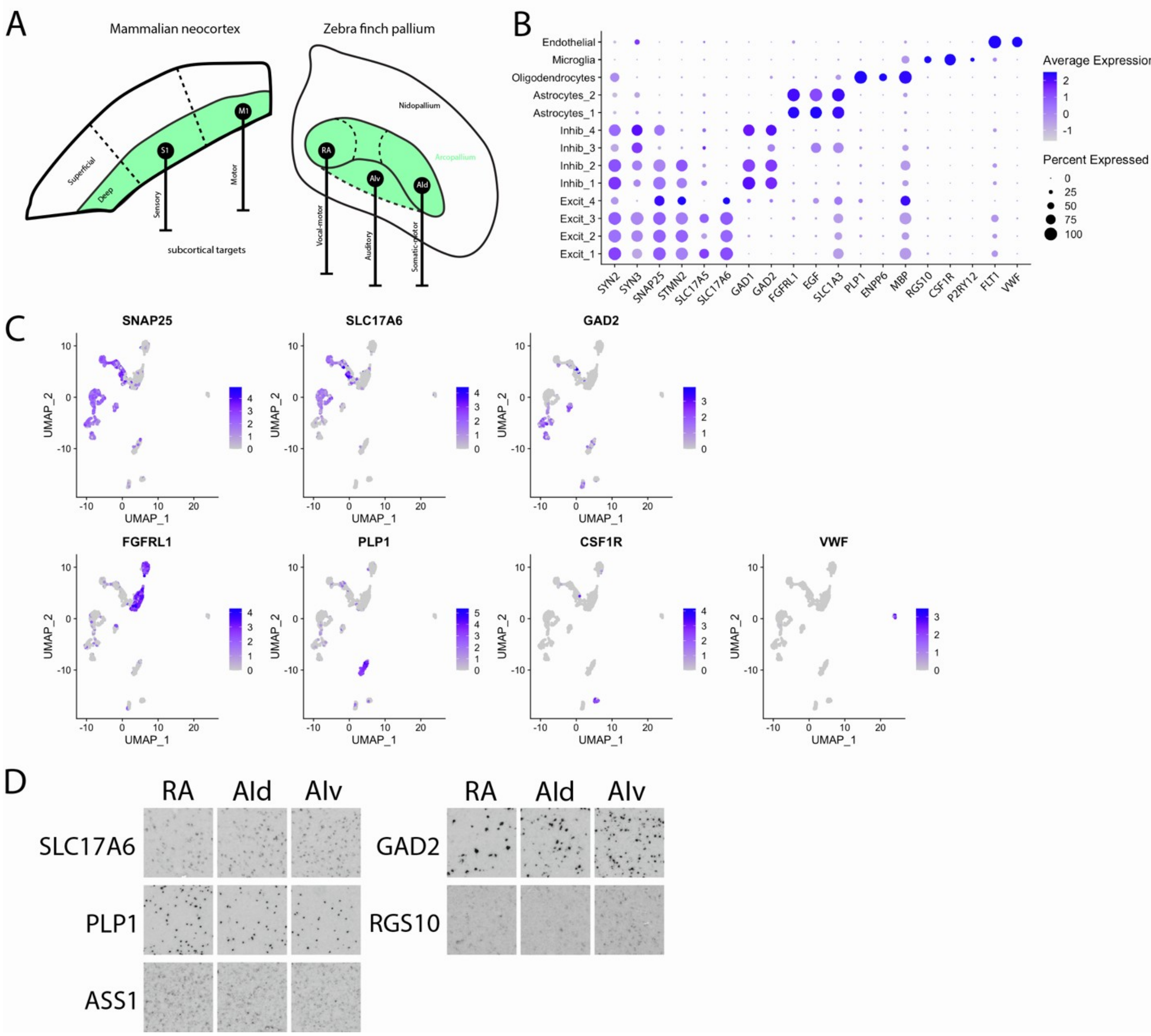

A
Mammalian neocortex
Zebra finch pallium
Superficial
Deep
S1
M1
Sensory
Motor
subcortical targets
Nidopallium
Arcopallium
RA
AIv
AId
Vocal-motor
Auditory
Somatic-motor
B
Endothelial
Microglia
Oligodendrocytes
Astrocytes_2
Astrocytes_1
Inhib_4
Inhib_3
Inhib_2
Inhib_1
Excit_4
Excit_3
Excit_2
Excit_1
SYN2 SYN3 SNAP25 STMN2 SLC17A5 SLC17A6 GAD1 GAD2 FGFRL1 EGF SLC1A3 PLP1 ENPP6 MBP RGS10 CSF1R P2RY12 FLT1 VWF
Average Expression
2
1
0
-1
Percent Expressed
0
25
50
75
100
C
SNAP25
SLC17A6
GAD2
FGFRL1
PLP1
CSF1R
VWF
UMAP_1
UMAP_2
D
RA
AId
AIv
SLC17A6
PLP1
ASS1
GAD2
RGS10

Figure S1: Defining cell types of the intermediate arcopallium (AI) of adult male zebra finches. Related to Figure 1.

(A) Schematic of comparison between descending somatic motor and sensory projections in the mammalian neocortex and the zebra finch AI.

(B) Expanded dot plot for cell type markers used for cell type annotation and in situ hybridization spatial investigation.

(C) UMAP plots for select markers that identify major cell types.

(D) High magnification images of cell type-defining markers shown in Figure 1E.

Figure S2

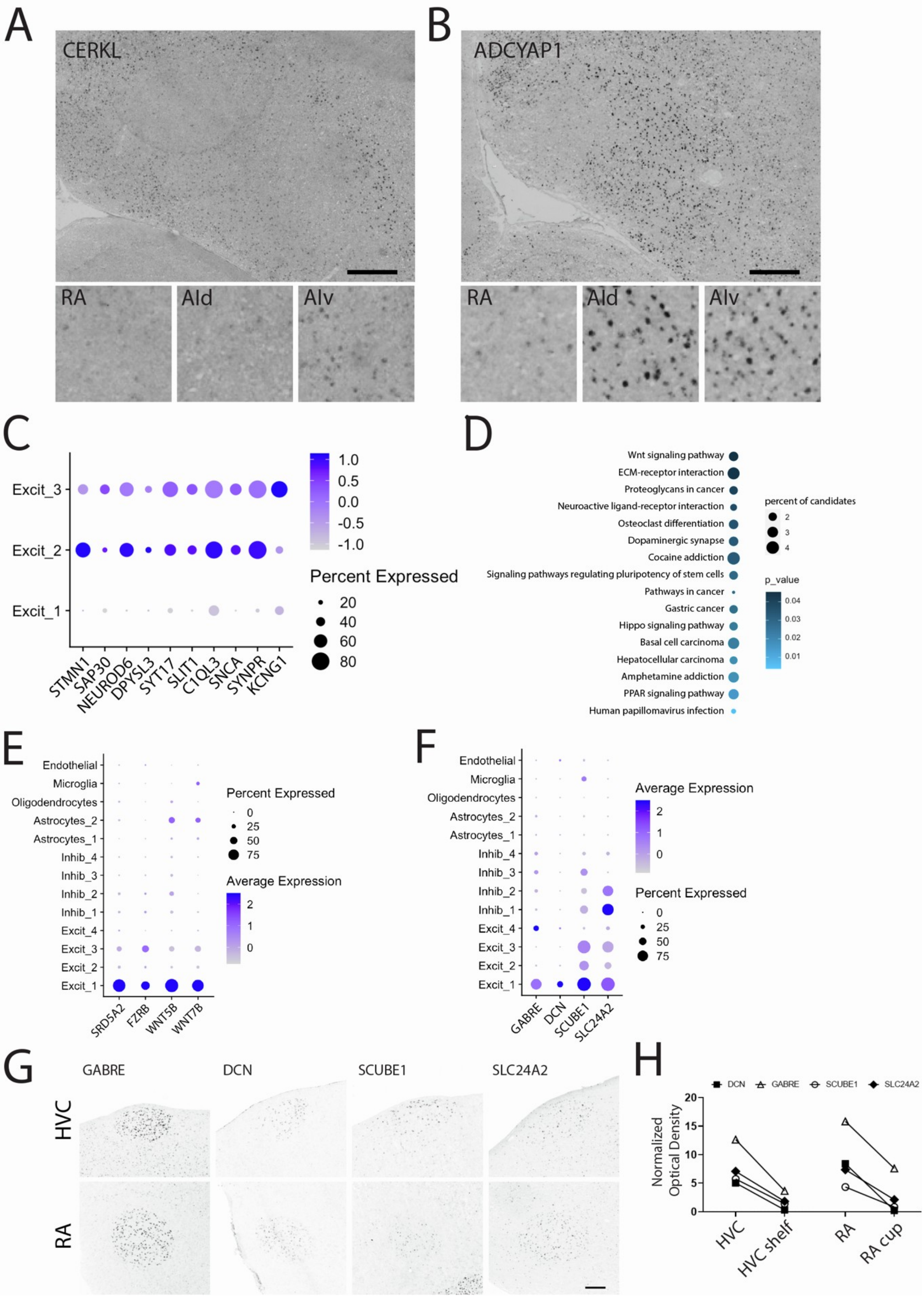
A
CERKL
RA
AId
AIv
B
ADCYAP1
RA
AId
AIv
C
Excit_3
Excit_2
Excit_1
STMN1
SAP30
NEUROD6
DPYSL3
SYT17
SLIT1
C1QL3
SNCA
SYNPR
KCNG1
1.0
0.5
0.0
-0.5
-1.0
Percent Expressed
20
40
60
80
D
Wnt signaling pathway
ECM-receptor interaction
Proteoglycans in cancer
Neuroactive ligand-receptor interaction
Osteoclast differentiation
Dopaminergic synapse
Cocaine addiction
Signaling pathways regulating pluripotency of stem cells
Pathways in cancer
Gastric cancer
Hippo signaling pathway
Basal cell carcinoma
Hepatocellular carcinoma
Amphetamine addiction
PPAR signaling pathway
Human papillomavirus infection
percent of candidates
2
3
4
p_value
0.04
0.03
0.02
0.01
E
Endothelial
Microglia
Oligodendrocytes
Astrocytes_2
Astrocytes_1
Inhib_4
Inhib_3
Inhib_2
Inhib_1
Excit_4
Excit_3
Excit_2
Excit_1
SRD5A2
FZRB
WNT5B
WNT7B
Percent Expressed
0
25
50
75
Average Expression
2
1
0
F
Endothelial
Microglia
Oligodendrocytes
Astrocytes_2
Astrocytes_1
Inhib_4
Inhib_3
Inhib_2
Inhib_1
Excit_4
Excit_3
Excit_2
Excit_1
GABRE
DCN
SCUBE1
SLC24A2
Average Expression
2
1
0
Percent Expressed
0
25
50
75
G
GABRE
DCN
SCUBE1
SLC24A2
HVC
RA
H
DCN
GABRE
SCUBE1
SLC24A2
Normalized Optical Density
20
15
10
5
0
HVC
HVC shelf
RA
RA cup

Figure S2: Excitatory neurons in RA and in the AI outside of RA. Related to Figure 2.

(A) An Excit_3 enriched gene (CERKL) has low expression in RA and AId, but higher expression in AIv, suggesting this cluster is AIv-biased. Scale bar is 400 µm.

(B) An Excit_2 marker (ADCYAP1) has low expression in RA but high expression in AId and AIv, suggesting this cluster identifies AI excitatory neurons that are absent or rare in RA. Scale bar is 400 µm.

(C) Dot plot of negative RA markers (listed on the ZEBrA website at www.zebrafinchatlas.org) [1] shows specificity for clusters Excit_2-3.

(D) ConsensusPathDB pathway analysis for cluster Excit_1 markers highlighting potential specialized pathways in RA.

(E) Dot plot of RA-specific gene (SRD5A2) and genes found in the Wnt:SFRP complex from the ConsensusPathDB analysis.

(F) Dot plot for four Excit_1 enriched genes with similar expression in RA and HVC.

(G) In situ hybridization for Excit_1 enriched genes that are shared markers of RA and HVC (shown are images from the ZEBrA website at www.zebrafinchatlas.org) [1]. Scale bar is 400 µm.

(H) Optical density measurements for the four RA/HVC markers showing enrichment compared to adjacent regions. Optical density measurements are normalized to background expression.

Figure S3

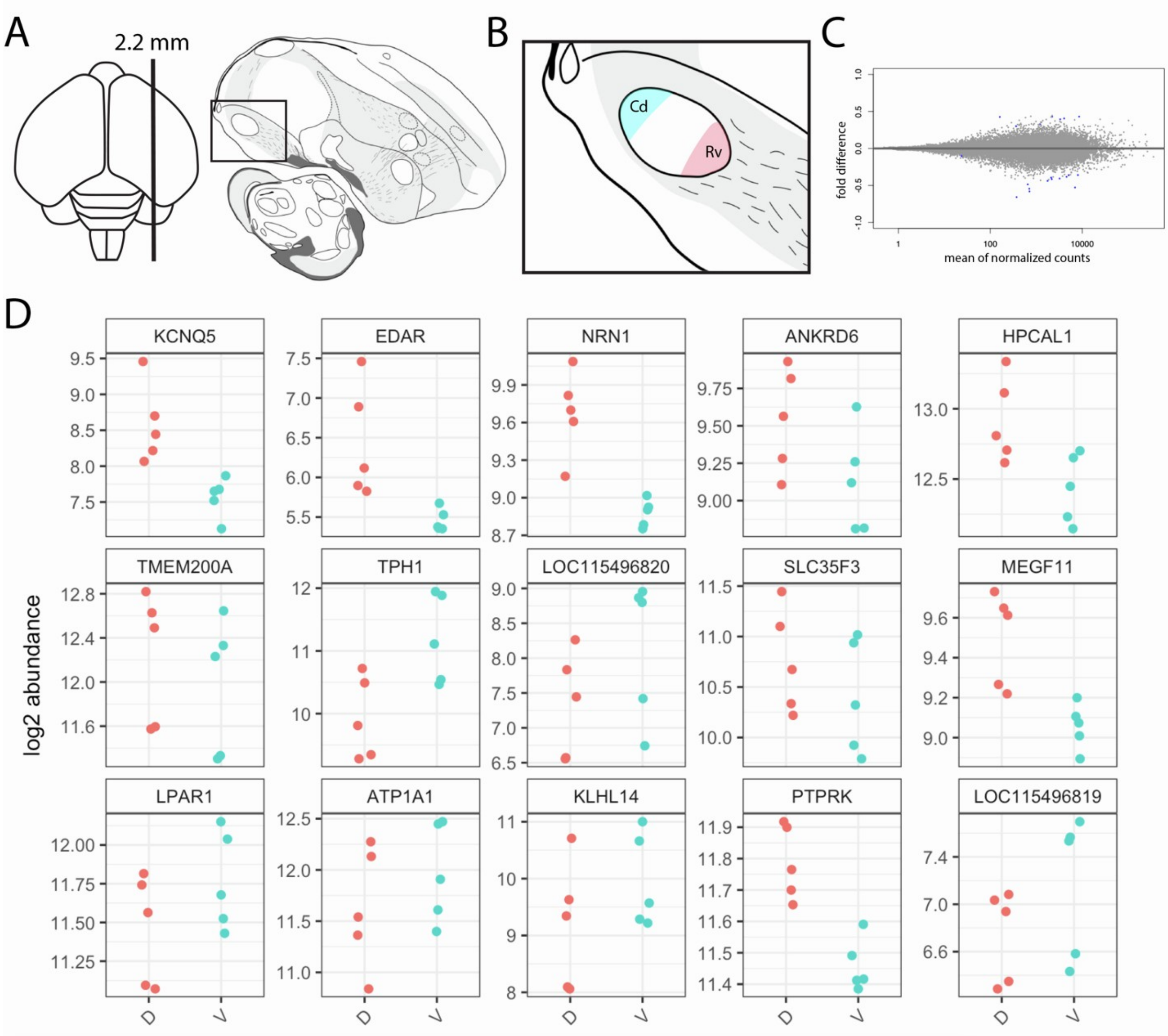
A
2.2 mm
B
Cd
Rv
C
fold difference
mean of normalized counts
D
log2 abundance
KCNQ5
EDAR
NRN1
ANKRD6
HPCAL1
TMEM200A
TPH1
LOC115496820
SLC35F3
MEGF11
LPAR1
ATP1A1
KLHL14
PTPRK
LOC115496819
D
V

Figure S3: Molecular homogeneity of RA. Related to Figure 2.

(A) Schematic dorsal view of zebra finch brain (left) representing the location of the parasagittal slice (right; drawing adapted from the ZEBrA website at www.zebrafinchatlas.org [1] and from [2]) used for microdissections; the area defined by the rectangle is shown in B.

(B) Location of the microdissections representing the Caudodorsal (Cd) and Rostroventral (Rv) divisions of RA used for bulk RNA-seq.

(C) Differential MA plot from bulk RNA-seq of Cd and Rv. Grey points indicate non-differential genes and blue points indicate significantly differential genes (FDR<0.05).

(D) Plots of transcript abundance in the caudodorsal and rostroventral regions for the 15 differential genes at FDR<0.05.

Figure S4

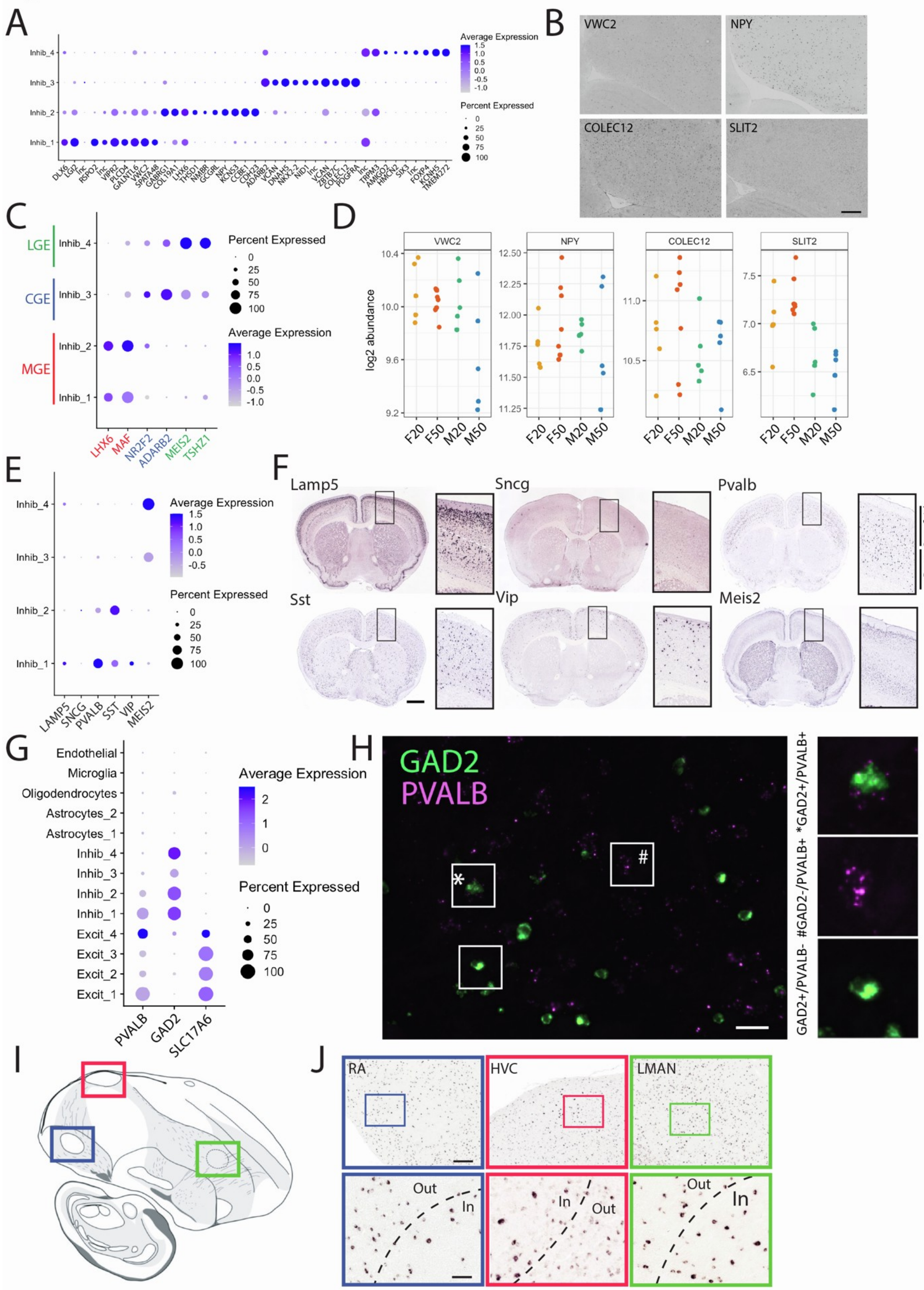
A
B
VWC2
NPY
COLEC12
SLIT2
Average Expression
Percent Expressed
C
LGE
CGE
MGE
Inhib_4
Inhib_3
Inhib_2
Inhib_1
LHX6
MAF
NR2F2
ADARB2
MEIS2
TSHZ1
D
log2 abundance
F20
F50
M20
M50
E
LAMP5
SNCG
PVALB
SST
VIP
MEIS2
F
Lamp5
Sncg
Pvalb
Superficial
Deep
Sst
Vip
Meis2
G
Endothelial
Microglia
Oligodendrocytes
Astrocytes_2
Astrocytes_1
Excit_4
Excit_3
Excit_2
Excit_1
GAD2
SLC17A6
H
GAD2
PVALB
*GAD2+/PVALB+
#GAD2-/PVALB+
GAD2+/PVALB-
I
J
RA
HVC
LMAN
Out
In

Figure S4: GABAergic cell subtypes in the AI. Related to Figure 3.

(A) Dot plot of the top 10 markers for each of the four AI inhibitory subtypes.

(B) In situ hybridization for proxy markers representing the four AI inhibitory subtypes: VWC2 (Inhib_1), NPY (Inhib_2), COLEC12 (Inhib_3), SLIT2 (Inhib_4). Scale bar is 400 µm.

(C) Dot plot of markers of medial, lateral, and caudal ganglionic eminence (MGE, LGE and CGE) suggests differential developmental origins of inhibitory subtypes.

(D) Age and sex effects on expression of inhibitory subtype proxy markers; bulk RNA-seq plots show a developmental decrease of VWC2 in males (log2FC of -0.57608 in M20-50) and SLIT2 was female biased at 50 dph.

(E) Dot plot shows differential expression of classical markers of mammalian cortical inhibitory subtypes across AI clusters.

(F) In situ hybridization for cortical inhibitory subtypes (images from the Allen Institute's Mouse Brain Atlas [3]); shown are screenshots of frontal sections, with the primary motor cortex expanded in the black rectangles. Scale bar is 1000 µm.

(G) Dot plot comparing the expression of PVALB with inhibitory (GAD2) and excitatory (SLC17A6) markers across AI clusters.

(H) Double fluorescence in situ hybridization of PVALB and GAD2 showing co-labeled cells (example denoted with *), as well as PVALB+/GAD2- (magenta, example denoted with #) and PVALB-/GAD2+ (green) cells in RA. Scale bar is 20 µm.

(I) Drawing of parasagittal section from adult male zebra finch (adapted from the ZEBrA website at www.zebrafinchatlas.org [1] and from [2]) highlighting the three pallial song nuclei. Scale bars are 400 µm (top) and 100 µm (bottom).

(J) GAD2 in situ hybridization images of RA, HVC, and LMAN (top); location of the images is indicated in I, according to color. Insets (bottom) show sparser, larger GAD2+ cells in RA and HVC compared to the adjacent areas. GAD2+ LMAN cells are of similar density compared to the surrounding nidopallium, with a subset being larger.

Figure S5

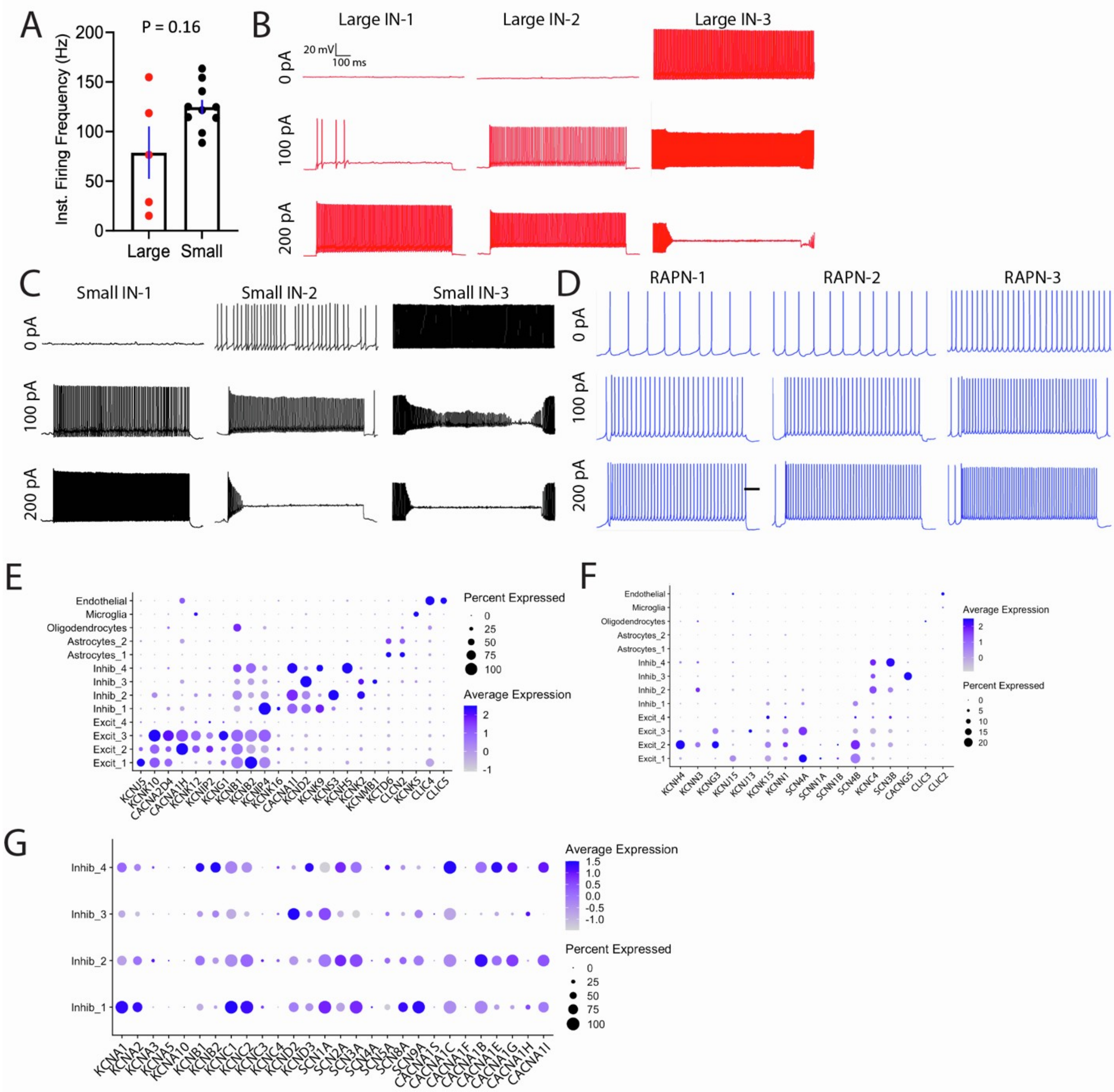
A
P = 0.16
Inst. Firing Frequency (Hz)
Large
Small
B
Large IN-1
Large IN-2
Large IN-3
20 mV
100 ms
0 pA
100 pA
200 pA
C
Small IN-1
Small IN-2
Small IN-3
D
RAPN-1
RAPN-2
RAPN-3
E
Percent Expressed
Average Expression
F
Average Expression
Percent Expressed
G
Average Expression
Percent Expressed

Figure S5: Recordings of mDlx+ neurons in RA and expression of intrinsic excitability genes in AI cell types. **Related to Figure 4.**

(A) Comparison of instantaneous firing frequencies of large (red) and small (black) cells; plotted are means +/- SEM, and individual values. Mann-Whitney U test, U = 13.

(B) Three large neurons with different spiking behaviors at 0 pA, +100 pA, and +200 pA current injections.

(C) Three small neurons with different spiking behaviors at 0 pA, +100 pA, and +200 pA current injections.

(D) Three examples of spiking behavior of RAPNs at 0 pA, +100 pA, and +200 pA current injection.

(E) Ion channel genes with high expression, across all AI cell types. Here and in panels (B-C) dot plots depict cell cluster distributions; shown are only genes with enriched expression in distinct clusters.

(F) Ion channel genes with high expression in few cells, across all AI cell types.

(G) Voltage-gated potassium channel subunits, voltage-gated sodium channel alpha subunits, and L-, N-, R-, and T-type calcium alpha subunits across inhibitory cell subtypes.

Figure S6

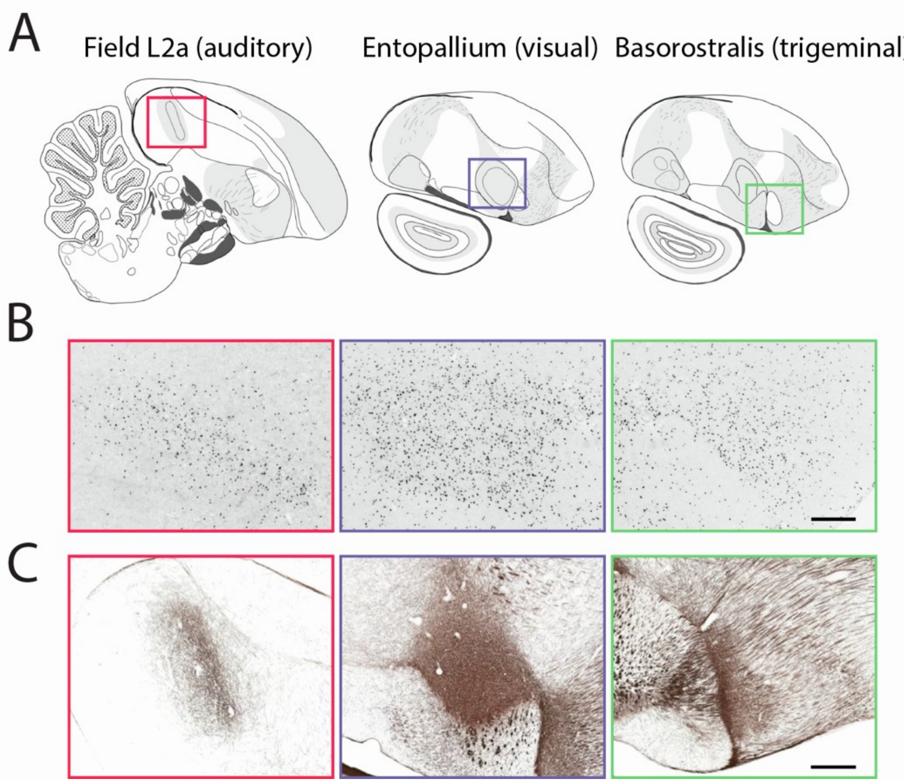
A
Field L2a (auditory)
Entopallium (visual)
Basorostralis (trigeminal)
B
C

Figure S6. Oligodendrocyte enrichment in avian analogs of mammalian layer 4 sensory cortices. Related to Figure 5.

(A) Drawings of serial parasagittal brain sections of adult male zebra finch (adapted from the ZEBrA website at www.zebrafinchatlas.org [1] and from [2]).

(B) Detailed views of in situ hybridization for PLP1 (from areas indicated by the colored rectangles in (A) show enrichment of oligodendrocytes in field L2a, entopallium and nucleus basorostralis. Scale bar is 800 µm.

(C) Views of myelin stain (images from the ZEBrA website at www.zebrafinchatlas.org [1] and from [2]) of the regions with high oligodendrocyte enrichment shown in A and B. Scale bar is 800 µm.

Figure S7

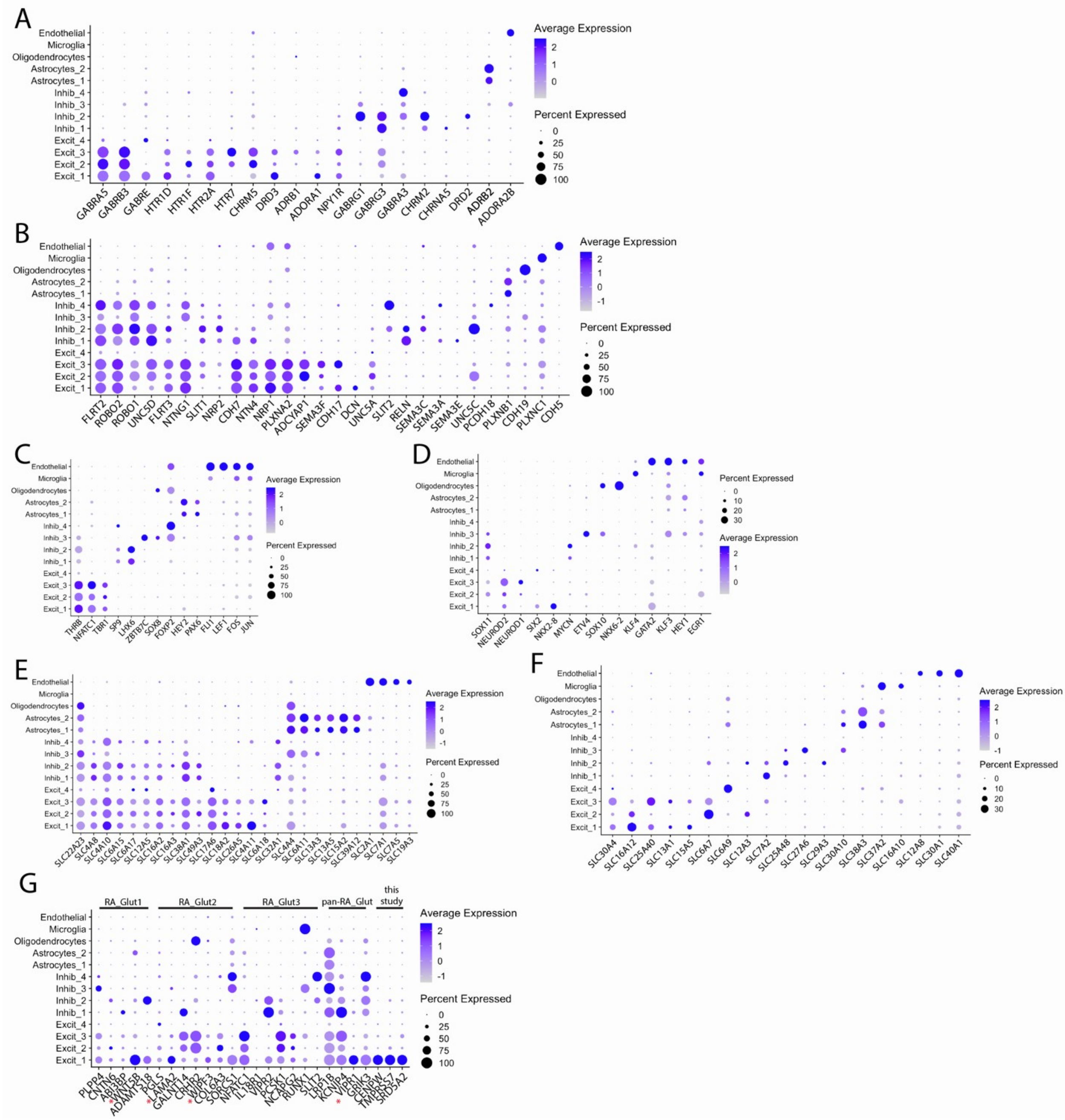

A
B
C
D
E
F
G
Endothelial
Microglia
Oligodendrocytes
Astrocytes_2
Astrocytes_1
Inhib_4
Inhib_3
Inhib_2
Inhib_1
Excit_4
Excit_3
Excit_2
Excit_1
Average Expression
Percent Expressed
GABRA5 GABRB3 GABRE HTR1D HTR1F HTR2A HTR7 CHRM5 DRD3 ADRB1 ADORA1 NPY1R GABRG1 GABRG3 GABRA3 CHRM2 CHRNA5 DRD2 ADRB2 ADORA2B
FLRT2 ROBO2 ROBO1 UNC5D FLRT3 NTNG1 SLIT1 NRP2 CDH7 NTN4 NRP1 PLXNA2 ADCYAP1 SEMA3F CDH17 DCN UNC5A SLIT2 RELN SEMA3C SEMA3A SEMA3E UNC5C PCDH18 PLXNB1 CDH19 PLXNC1 CDH5
THRB NFATC1 TBR1 SP9 LHX6 ZBTB7C SOX8 FOXP2 HEY2 PAX6 FLI1 LEF1 FOS JUN
SOX11 NEUROD2 NEUROD1 SIX2 NKX2-8 MYCN ETV4 SOX10 NKX6-2 KLF4 GATA2 KLF3 HEY1 EGR1
SLC22A23 SLC4A8 SLC4A10 SLC6A15 SLC6A17 SLC12A5 SLC16A2 SLC16A3 SLC38A1 SLC49A3 SLC17A6 SLC18A2 SLC26A5 SLC4A11 SLC6A18 SLC32A1 SLC4A4 SLC6A11 SLC13A3 SLC13A5 SLC15A2 SLC39A12 SLC2A1 SLC7A1 SLC7A5 SLC19A3
SLC30A4 SLC16A12 SLC25A40 SLC13A1 SLC15A5 SLC6A7 SLC6A9 SLC12A3 SLC7A2 SLC25A48 SLC27A6 SLC29A3 SLC30A10 SLC38A3 SLC37A2 SLC16A10 SLC12A8 SLC30A1 SLC40A1
RA_Glut1
RA_Glut2
RA_Glut3
pan-RA_Glut
this study

Figure S7: Molecular analysis of physiologically relevant gene families in AI cell types. Related to Table S1.

(A) Neurotransmitter and neuromodulator receptor genes. Here and in all other panels dot plots depict cell cluster distributions; shown here and in panels (B-F) are only genes with enriched expression in distinct clusters.

(B) Axon guidance related genes.

(C) Transcription factor genes with high expression.

(D) Transcription factor genes with high expression in few cells.

(E) Solute carrier genes with high expression.

(F) Solute carrier genes with genes with high expression in few cells.

(G) Mapping genes linked to the three molecularly distinct excitatory clusters (RA_Glut1-3) defined in Colquitt et al. [4] onto clusters from our dataset. Most are not specific to RA (i.e. markers not unique to Excit_1, which is unique to RA – see "this study" markers - and/or also present or enriched in Excit_2/3, which are sparse or absent in RA) or not specific to RA excitatory cells (i.e. also present in inhibitory neurons and/or non-neuronal cells). Red asterisks denote qualitatively unique expression in RA excitatory neurons.

1. Lovell, P.V., Wirthlin, M., Kaser, T., Buckner, A.A., Carleton, J.B., Snider, B.R., McHugh, A.K., Tolpygo, A., Mitra, P.P., and Mello, C.V. (2020). ZEBrA: Zebra finch Expression Brain Atlas-A resource for comparative molecular neuroanatomy and brain evolution studies. J Comp Neurol 528, 2099-2131. 10.1002/cne.24879.
2 Karten H.J., Brzozowska-Prechtl A., Lovell P.V., Tang D.D., Mello C.V., Wang H., Mitra P.P. Digital atlas of the zebra finch (Taeniopygia guttata) brain: a high-resolution photo atlas. J. Comp. Neurol. 2013;521:3702–3715. doi:10.1002/cne.23443.
3. Lein E.S., Hawrylycz M.J., Ao N., Ayres M., Bensinger A., Bernard A., Boe A.F., Boguski M.S., Brockway K.S., Byrnes E.J., et al. Genome-wide atlas of gene expression in the adult mouse brain. Nature 2007;445:168–176. doi:10.1038/nature05453.
4. Colquitt, B.M., Merullo, D.P., Konopka, G., Roberts, T.F., and Brainard, M.S. (2021). Cellular transcriptomics reveals evolutionary identities of songbird vocal circuits. Science 371. 10.1126/science.abd9704.